Paleoceanography and Paleoclimatology

RESEARCH ARTICLE
10.1029/2018PA003472

Key Points:
- Deep waters sourced in the Pacific sector of Southern Ocean (SO) maintained high $\delta^{13}C$ values throughout the last 800 kyr
- A spatial gradient in SO-sourced deep water $\delta^{13}C$ was present between the Atlantic and Pacific SO throughout much of the Late Quaternary
- Differing methods of AABW formation are invoked to explain the observed difference in deep water $\delta^{13}C$ within the SO

Supporting Information:
- Supporting Information S1
- Supporting Information S2
- Figure S1
- Figure S2
- Figure S3
- Figure S4
- Table S1
- Data Set S1
- Data Set S2

Correspondence to:
T. J. Williams and C.-D. Hillenbrand,
thomas.williams@ufl.edu;
hilc@bas.ac.uk

Citation:
Williams, T. J., Hillenbrand, C.-D., Piotrowski, A. M., Allen, C. S., Frederichs, T., Smith, J. A., et al. (2019). Paleocirculation and ventilation history of Southern Ocean sourced deep water masses during the last 800,000 years. *Paleoceanography and Paleoclimatology*, *34*, 833–852. https://doi.org/10.1029/2018PA003472

Received 30 AUG 2018
Accepted 16 APR 2019
Accepted article online 25 APR 2019
Published online 22 MAY 2019

Paleocirculation and Ventilation History of Southern Ocean Sourced Deep Water Masses During the Last 800,000 Years

Thomas J. Williams[1,2,3], Claus-Dieter Hillenbrand[2], Alexander M. Piotrowski[3], Claire S. Allen[2], Thomas Frederichs[4], James A. Smith[2], Werner Ehrmann[5], and David A. Hodell[3]

[1]Department of Geological Sciences, University of Florida, Gainesville, FL, USA, [2]British Antarctic Survey, Cambridge, UK, [3]Department of Earth Sciences, Cambridge University, Cambridge, UK, [4]Faculty of Geosciences, University of Bremen, Bremen, Germany, [5]Institute for Geophysics and Geology, University of Leipzig, Leipzig, Germany

Abstract Most conceptual models of ocean circulation during past glacial periods invoke a shallowed North Atlantic-sourced water mass overlying an expanded, poorly ventilated Southern Ocean (SO)-sourced deep water mass (Southern Component Water or SCW), rich in remineralized carbon, within the Atlantic basin. However, the ventilation state, carbon inventory, and circulation pathway of SCW sourced in the Pacific sector of the SO (Pacific SO) during glacial periods are less well understood. Here we present multiproxy data—including $\delta^{18}O$ and $\delta^{13}C$ measured on the benthic and planktic foraminifera *Cibicidoides wuellerstorfi*, and *Neogloboquadrina pachyderma*, and productivity proxies including percent $CaCO_3$, total organic carbon, and Ba/Ti—from a sediment core located in the high-latitude (71°S) Pacific SO spanning the last 800 kyr. Typical glacial $\delta^{13}C$ values of SCW at this core site are ~0‰. We find no evidence for SCW with extremely low $\delta^{13}C$ values during glacials in the high-latitude Pacific SO. This leads to a spatial gradient in the stable carbon isotope composition of SCW from the high-latitude SO, suggesting that there are different processes of deep- and bottom-water formation around Antarctica. A reduced imprint of air-sea gas exchange is evident in the SCW formed in the Atlantic SO compared with the Pacific SO. A spatial $\delta^{13}C$ gradient in SCW is apparent throughout much of the last 800,000 years, including interglacials. A SO-wide depletion in benthic $\delta^{13}C$ is observed in early MIS 16, coinciding with the lowest atmospheric pCO_2 recorded in Antarctic ice cores.

1. Introduction

Reconstructed seawater carbonate ion concentrations and $\delta^{13}C$ recorded in tests of the benthic foraminifera *Cibicidoides* spp. ($\delta^{13}C_{cib}$) demonstrate that a sharp chemical boundary existed between North-Atlantic source waters (Northern Component Water, NCW) and Southern Ocean (SO)-sourced waters (Antarctic Bottom Water [AABW]/Lower Circumpolar Deep Water [LCDW]; collectively, these ancient water masses are hereafter referred to as Southern Component Water, SCW) in the glacial Atlantic Ocean (Curry & Oppo, 2005; Peterson et al., 2014; Yu et al., 2016). This vertical chemical gradient has been identified during multiple glacials (Hodell et al., 2003; Oliver et al., 2010) and is thought to reflect increased physical stratification within the Atlantic Ocean, with well-ventilated NCW overlying poorly ventilated SCW rich in remineralized carbon (Ferrari et al., 2014; Freeman et al., 2016; Gebbie, 2014; Lund et al., 2011; Lynch-Stieglitz et al., 2007). Temperature and salinity reconstructions suggest that this stratification was established and maintained via an increase in the salinity of SCW below this chemical divide (Adkins et al., 2002; Roberts et al., 2016). The shoaling of the NCW-SCW boundary to depths above rough bathymetry is also hypothesized to have reduced turbulent mixing between these water masses (Ferrari et al., 2014). During glacials, this reduced mixing between SCW and NCW, coupled with a more vigorous sequestration of carbon via the biological pump, is thought to have driven down pCO_2^{atm} (Adkins et al., 2002; Archer et al., 2003; Curry & Oppo, 2005; Hoogakker et al., 2015; Jaccard et al., 2016; Yu et al., 2008, 2016). The subsequent breakdown of this stratification during glacial terminations led to the release of large amounts of this stored carbon back into the atmosphere, helping to drive a rapid transition from glacial to interglacial states (Anderson et al., 2009; Schmitt et al., 2012).

Reconstructed seawater dissolved inorganic carbon (DIC) $\delta^{13}C$ values in the abyssal South Atlantic and Atlantic sector of the SO (hereafter Atlantic SO: >30°S, 70°W to 50°E) reached <-1‰ during the last glacial period, the lowest in the global ocean. A northward gradient toward higher $\delta^{13}C_{cib}$ values within the deep Atlantic basin (Curry & Oppo, 2005; Gebbie et al., 2015) points to SCW formation in the Atlantic SO as the source of these poorly ventilated, low $\delta^{13}C$ deep waters. Paleocirculation pathways and past distribution of seawater $\delta^{13}C$ values outside of the Atlantic and Atlantic SO are currently less well constrained, however. A compilation of global $\delta^{13}C_{cib}$ values from the Last Glacial Maximum (LGM; approximately 18–24 ka) shows no evidence for extremely low (<-1‰) $\delta^{13}C$ values in the Pacific basin during the LGM (Peterson et al., 2014); however, data coverage is sparse compared with the Atlantic. While lower than modern values, LGM $\delta^{13}C_{cib}$ in the Southern Pacific and Pacific sector of the SO (hereafter Pacific SO: >30°S, 165°E to 70°W) were not as low as the Atlantic SO (Bostock et al., 2013). Studies of LGM $\delta^{13}C_{ib}$ depth profiles from core sites located within the SW Pacific have demonstrated a middepth 'bulge' of ^{13}C depleted waters (McCave et al., 2008; Sikes et al., 2017), with a $\delta^{13}C_{cib}$ minimum of ~ -0.5‰ centered around approximately 2,500- to 3,000-m water depth, and elevated values above and below this depth. The depth of this $\delta^{13}C_{cib}$ minimum in the SW Pacific coincides with maxima in oxygen isotope values of benthic foraminifera shells ($\delta^{18}O_{cib}$) and maximum radiocarbon ventilation ages within the Pacific SO, perhaps reflecting reduced entrainment of NCW within the SO at this time (Bostock et al., 2013; McCave et al., 2008; Ronge et al., 2016; Sikes et al., 2016; Skinner et al., 2017). In places, abyssal waters within the glacial Pacific SO appear to have remained better ventilated than within both the middepth Pacific SO and the abyssal Atlantic SO suggesting admixture of a better ventilated bottom water mass between the Atlantic and the Pacific (Sikes et al., 2017), presumably sourced in the high-latitude Pacific SO. However, $\delta^{13}C_{cib}$ records from the high-latitude Pacific SO spanning the last glacial period with which to test this hypothesis are currently unavailable. There is also a paucity of $\delta^{13}C_{cib}$ records spanning multiple glacial cycles with which to further examine glacial-interglacial variability in high-latitude SO paleocirculation. In this study, we use $\delta^{13}C_{cib}$ alongside other proxies from marine sediment core PC493, located at 71°S within the Pacific SO, to better constrain temporal variations in $\delta^{13}C$ of SCW within the Pacific SO, and examine SO paleocirculation pathways and methods of deep water formation across the late Quaternary.

2. Materials and Methods

2.1. Hydrographic and Sedimentological Setting

Piston core PC493 (71°07′50″S, 119°54′49″W, 2,077-m water depth, 10.4-m recovery of which 2.87 m is presented here) was retrieved from the West Antarctic continental slope in the Pacific SO during cruise JR179 aboard RRS *James Clark Ross* in 2008 (Figure 1). This core site is located on an isolated plateau atop a seamount belonging to the Marie Byrd Seamounts in the Amundsen Sea, a location previously reported to contain abundant calcareous foraminifera (cf. core PS2547 from the same site; see Hillenbrand et al., 2002). The position of site PC493 atop a seamount means the sediments of PC493 have remained undisturbed from the effects of turbidites (which have affected portions of nearby sediment cores; for example, Hillenbrand et al., 2002), and the core is free of major hiatuses. The sediments comprise a condensed but continuous sequence of olive brown, foraminiferal oozes, muds, and foraminifera-bearing muds (Figure 2). The presence of muds suggests a lack of current winnowing at this site, and the amount of biogenic versus lithogenic clasts broadly follows glacial-interglacial cyclicity with reduced biogenic clasts during glacial periods (Figure 2). Situated close to the modern maximum summer (February) sea-ice limit (Jacka, 1997), site PC493 is today bathed in LCDW as it upwells along the Antarctic continental margin, south of the southern boundary of the clockwise flowing Antarctic Circumpolar Current (ACC; Orsi et al., 1995; Figure 1b). In the modern SO, LCDW is predominantly a mixture of circumpolar waters with components of North Atlantic Deep Water (NADW) and AABW. The presence of NADW is reflected by a salinity maximum in LCDW most prominent in the Atlantic SO and Indian SO (defined here as 50°E to 165°E). Intensive mixing within the ACC leads to LCDW with more uniform physical properties within the Pacific SO compared with the Atlantic SO and Indian SO (Figure 1c). Reconstructions of near-surface water oxygen concentrations show that upwelling of deep water has continued at site PC493 throughout at least the last 250 kyr (Lu et al., 2016). As its location lies 'upstream' of the main inflow of Pacific Deep Water (PDW; poorly oxygenated waters in Figure 1b) into the SO, which mixes with Circumpolar Deep Water (CDW) within the ACC in the central

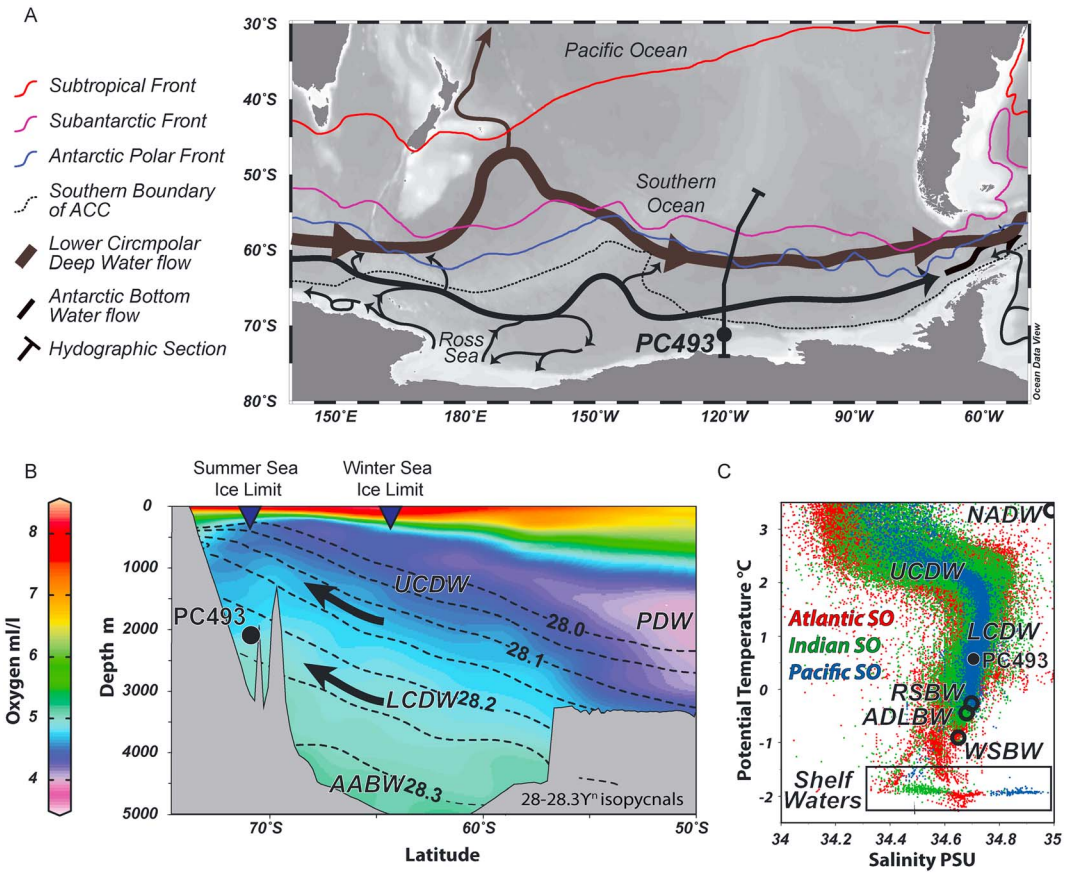

Figure 1. Location of sediment core PC493 together with Southern Ocean (SO) hydrographic data. (a) Schematic deep and bottom water circulation in the Pacific SO. The thick lines denote major interbasin circulation pathways, and the thin arrows denote intrabasin circulation pathways (Morozov et al., 2010; Orsi et al., 1999). (b) Hydrographic section across site PC493 showing oxygen content and lines of neutral density, demonstrating the upwelling of deep- and bottom-water masses in the Pacific SO. The location of this section is shown in panel (a). (c) Potential temperature and salinity of waters bathing site PC493 in relation to water masses of >500-m water depth in the SO, including Ross Sea Bottom Water (RSBW), Adélie Land Bottom Water (ADLBW), Weddell Sea Bottom Water (WSBW), Lower and Upper Circumpolar Deep Water (LCDW/UCDW), and North Atlantic Deep Water (NADW) as it enters the SO (Martinson et al., 2008; Pardo et al., 2012). Data from the Atlantic (70°W to 50°E), Indian (50°E to 165°E), and Pacific (165°E to 70°W) SO are differentiated. All plots created using Ocean Data View (Schlitzer, 2015), using data from the Hydrographic Atlas of the Southern Ocean (panel b; Olbers et al., 1992) and the World Ocean Atlas 2013 (panel c; Garcia et al., 2014).

and eastern Pacific SO (Talley, 2013), core PC493 is well situated to monitor the carbon isotope composition of SCW in the high-latitude Pacific SO.

2.2. Stable Carbon and Oxygen Isotope Analyses

Stable carbon and oxygen isotope analyses were performed on the planktic foraminifer species *Neogloboquadrina pachyderma* sinistral (12–24 tests) and the epibenthic foraminifer *Cibicidoides wuellerstorfi* (5–20 tests). Tests were picked from the wet sieved 63- to 2,000-μm sediment size fraction at every centimeter of the upper 2.87 m of core PC493 and analyzed at the Godwin Laboratory for Palaeoclimate Research at the Department of Earth Sciences, University of Cambridge (UK), using a Micromass Multicarb sample preparation system attached to a VG SIRA Mass Spectrometer. Results are reported with reference to the international standard Vienna Pee Dee Belemnite, and analytical precision is better than +/- 0.06‰ for $\delta^{13}C$ and +/-0.08‰ for $\delta^{18}O$.

Multiple studies have demonstrated that of all benthic foraminifer taxa, *C. wuellerstorfi* forms its tests closest to equilibrium with $\delta^{13}C$ of seawater DIC and is therefore the preferred benthic species for $\delta^{13}C$ reconstructions (Belanger et al., 1981; Duplessy et al., 1984; Graham et al., 1981; Mix et al., 1991; Schmittner et al., 2017; Woodruff et al., 1980). In contrast, the $\delta^{13}C$ values of *N. pachyderma* sin. ($\delta^{13}C_p$) in the high-latitude SO display an offset from the equilibrium with $\delta^{13}C$ DIC values of surface water. The offset between core-top

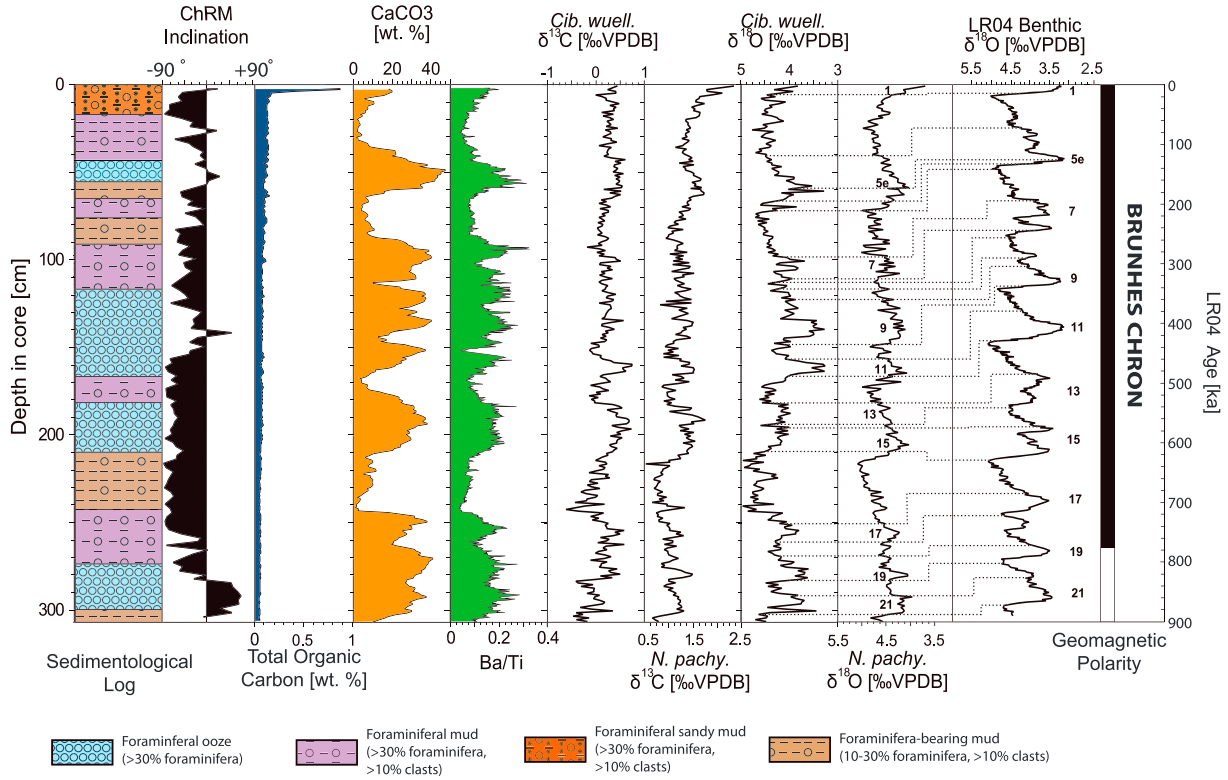

Figure 2. Lithology, inclination of the Characteristic Remanent Magnetization (ChRM) with magnetic polarity, paleoproductivity proxies (total organic carbon [TOC], $CaCO_3$ content, and Barium/Titanium [Ba/Ti] ratio), and $\delta^{13}C$ and $\delta^{18}O$ isotope data measured on planktic (*Neogloboquadrina pachyderma* sinistral) and benthic (*Cibicidoides wuellerstorfi*) foraminifera from core PC493. The LR04 benthic $\delta^{18}O$ stack (Lisiecki & Raymo, 2005) with numbers giving interglacial Marine Isotope Stages and age-depth tie points (indicated by dotted lines) is also shown. Note that the analysis made on core PC493 is on a depth scale (left axis), while the LR04 stack and global geomagnetic polarity are plotted versus age (right axis).

N. pachyderma sin. and modeled preindustrial equilibrium seawater $\delta^{13}C$ values has been shown to increase from approximately 1‰ at 70°S to approximately1 2.8‰ at 43°S in the Atlantic SO (Charles & Fairbanks, 1990; Kohfeld et al., 2000). The variable offset is the result of changes in (i) dietary $\delta^{13}C$, (ii) seawater carbonate ion concentrations, and (iii) seawater temperature. Based on the modeled preindustrial offset from equilibrium surface waters at 70°S (Kohfeld et al., 2000), a correction of +1.0‰ is applied to all $\delta^{13}C_p$ data presented here.

$\delta^{18}O$ measured on *C. wuellerstorfi* tests ($\delta^{18}O_{cib}$) does not match equilibrium seawater $\delta^{18}O$, and an offset of 0.64‰ has been suggested to correct for vital effects (Shackleton, 1974), although this may be an over estimate and may not be uniform in all ocean basins (Keigwin, 1998; Marchitto et al., 2014). The vital offset for *N. pachyderma* sin. $\delta^{18}O$ ($\delta^{18}O_p$) is not well constrained, with estimates ranging from 0.5 to 1.5‰ (Hendry et al., 2009; Pados et al., 2015). The range in these estimates may reflect variable calcification depths within the upper approximately 20–200 m of the water column (Kohfeld et al., 1996), where fluctuations in temperature and salinity could result in variable $\delta^{18}O$ values of calcite within the life cycle of a single foraminifer. On the other hand, there is evidence that *N. pachyderma* sin. migrates vertically within the water column to maintain constant temperature and salinity conditions (Simstich et al., 2003). Neither benthic nor planktic $\delta^{18}O$ data of core PC493 presented here have been corrected for these offsets.

2.3. Barium/Titanium (Ba/Ti) Ratios, Total Organic Carbon (TOC), and $CaCO_3$ Contents

The barium/titanium (Ba/Ti) ratio of sediments reflects the content of biogenic barium, which is the most reliable productivity proxy in sediments from the Antarctic continental margin (Bonn et al., 1998; Hillenbrand et al., 2002, 2009) and south of the Antarctic Polar Front (APF; Jaccard et al., 2013; Nürnberg et al., 1997). Ba/Ti ratios were measured to gauge the potential for past biological productivity changes to

affect $\delta^{13}C_{cib}$ at site PC493 (Mackensen et al., 1993). X-ray fluorescence (XRF) scanning of sediment core PC493 was undertaken to obtain semiquantative Ba and Ti concentrations. The split archive halves of core PC493 were analyzed using an Avaatech XRF core scanner at the Department of Earth Sciences, University of Cambridge (UK), to obtain elemental data at 2.5-mm spatial resolution. The length and width of the irradiated surface was 10 and 12 mm. The detector consisted of the Canberra X-PIPS Silicon Drift Model SXD 15C-150-500 with 150eV X-ray resolution and the Canberra Digital Spectrum Analyzer 1000. Spectra was fit with WinAxil software.

The calcium carbonate ($CaCO_3$) content of marine sediments is controlled by productivity of calcareous (mainly planktic) microfossils, carbonate dissolution, and dilution by noncalcareous sediment components. Dissolution has been shown to cause an offset between $\delta^{13}C$ recorded in foraminiferal calcite and that of seawater DIC (McCorkle et al., 1995). The $CaCO_3$ content of core PC493 was also measured in order to (a) assess changes in productivity and (b) monitor for potential dissolution of $CaCO_3$. Total carbon (TC) content was first determined on ground bulk sediment samples using a Vario EL III Elementar analyzer at the Institute for Geophysics and Geology, University of Leipzig (Germany). TOC was measured with an Eltra METALYST-CS-1000-S after removal of the inorganic carbon with HCl, and $CaCO_3$ contents were calculated from the TC and TOC data.

3. Results

3.1. Stable Oxygen Isotopes, Age Model, and Sedimentation Rates

Both $\delta^{18}O_p$ and $\delta^{18}O_{cib}$ demonstrate cyclical variations, which reflect changes in temperature and the $\delta^{18}O$ of seawater, which on the timescales discussed here is predominantly influenced by global ice volume. The age model for core PC493 is also constrained by the presence of the Bruhnes-Matuyama boundary (780 ka), inferred from the ChRM Inclination reversal at 277- to 284-cm core depth (Figure 2), which occurs in Marine Isotope Stage (MIS) 19. The age model was refined via tuning of both $\delta^{18}O_p$ and $\delta^{18}O_{cib}$ data to the LR04 global $\delta^{18}O_{cib}$ stack (Lisiecki & Raymo, 2005). $\delta^{18}O_{cib}$ age-depth tie points for core PC493 were mainly taken as the transition between glacial and interglacial MIS as defined by the LR04 stack (Lisiecki & Raymo, 2005). Other tie points, such as the interglacial MIS 5e $\delta^{18}O$ minimum at 123 ka (Lisiecki & Raymo, 2005) and the glacial MIS 8 $\delta^{18}O$ peak at 294 ka (cf. substage 8.6 of Imbrie et al., 1984), were also used (Figure 2). A full list of tie points is provided in Table S1 in the supporting information. Sedimentation rates at site PC493 were generally low throughout the last 800 kyr, averaging 0.36 cm/kyr (Figure 3), providing an average sampling resolution of ~3 kyr for stable isotopic analyses.

$\delta^{18}O_{cib}$ values do not match the maxima/minima of the LR04 stack for every glacial/interglacial of the last 800 kyr, suggesting some smoothing of the $\delta^{18}O_{cib}$ record, probably due to the low sedimentation rates. Between ~65 and 90% of the expected glacial-interglacial $\delta^{18}O_{cib}$ variability found in the LR04 stack is observed at site PC493 (Figures 3 and S1 in the supporting information). Bioturbation is likely to have been minimal at this site given the low TOC contents of the sediments (section 3.3. and Figure 2), which probably inhibited the establishment of a significant benthic community at this location, as exemplified by the lack of infaunal foraminifera species such as *Uvigerina*. Nevertheless, it has to be taken into account that our isotope data were derived from a 1-cm-thick sediment slice representing a few kiloyears, that is, our data are likely to present an integrated, and thus somewhat smoothed, isotope signal. Termination 1 (TI) appears to be diffuse in the $\delta^{18}O_b$ record of PC493, which may reflect either bioturbation or coring disturbance of the upper few centimeter of the core. Stable oxygen isotope data from trigger core TC493 retrieved alongside piston core PC493 do not show the same 'smearing' through TI (Lu et al., 2016), and $\delta^{18}O$ and $\delta^{13}C$ data from the LGM and deglacial sections of TC493 are therefore presented here alongside the record of PC493 (hereafter TPC493 when referring to both records).

3.2. Stable Carbon Isotopes

The $\delta^{13}C_{cib}$ values of core PC493 typically range from 0.5 to 0.7‰ during peak interglacials and from -0.2 to 0.2‰ during glacial maxima (Figure 3). The amplitude of $\delta^{13}C_{cib}$ changes at glacial terminations varies between 0.7‰ and 0.2‰, with an average amplitude of 0.39±0.16‰ across all terminations. The $\delta^{13}C_{cib}$ record of TC493 shows an increase of approximately 0.42‰ between the LGM (18–24 ka average $\delta^{13}C_{cib}$= 0.29‰, σ=0.16‰) and the early Holocene (9.5-8 ka average $\delta^{13}C_{cib}$= 0.71‰, σ=0.21‰), close to the

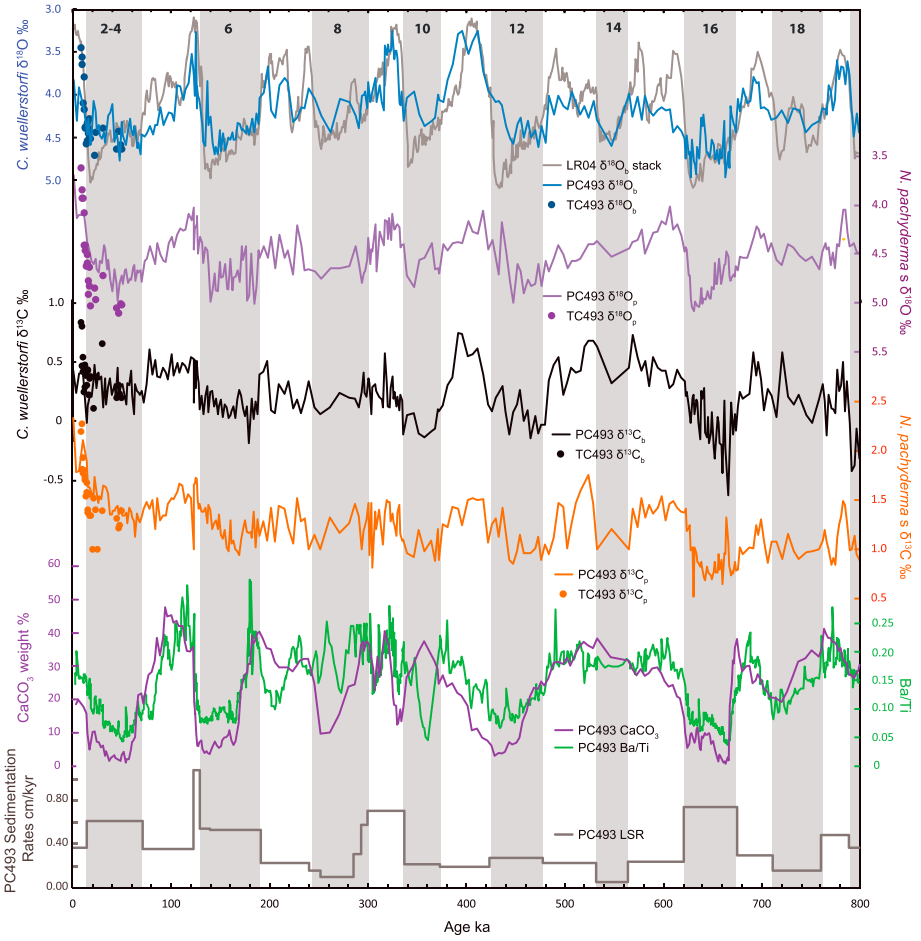

Figure 3. Proxy records at site PC493. Stable isotope records of piston core PC493 and associated trigger core TC493 (dots) measured on benthic *Cibicidoides wuellerstorfi* and planktic *Neogloboquadrina pachyderma* (s) tests, alongside the LR04 $\delta^{18}O_b$ stack (grey curve; Lisiecki & Raymo, 2005) and palaeoproductivity indicators $CaCO_3$ content and Ba/Ti ratio. Also shown are linear sedimentation rates (LSRs) for core PC493. At no point during the last 800 kyr did $\delta^{13}C_{cib}$ values in core PC493 (or core its trigger core, TC493) reach the extreme values (<-1.0‰) found in sediment cores from the deep South Atlantic and Atlantic Southern Ocean during past glacial periods. Glacial Marine Isotope Stages are shaded and numbered according to Lisiecki and Raymo (2005).

0.38±0.08‰ whole ocean (0.5–5 km water depth) $\delta^{13}C$ shift across the last deglaciation estimated by Peterson et al. (2014). The LGM $\delta^{13}C_{cib}$ minimum in core TC493 was 0.11‰.

$\delta^{13}C_p$ values in core PC493 range from 1.3 to 1.7‰ during peak interglacials and from 0.8 to 1.2‰ during glacial maxima, while the amplitude across terminations varies from 0.2 to 0.6‰. The average amplitude in $\delta^{13}C_p$ values across all terminations is 0.43±0.11‰. The $\delta^{13}C_p$ values in core PC493 are higher in the Holocene than at any other point during the last 800 kyr, with peaks of 2.33‰ (0.5 cm) and 2.11‰ (4.5 cm) being particularly high.

Despite the low sedimentation rates at site PC493, there is no consistent relationship between lower (glacial) or higher (interglacial) $\delta^{13}C_{cib}$ values and higher sedimentation rates (Figure 3), as might be expected if the $\delta^{13}C_{cib}$ record had been significantly smoothed by either integrating isotopic signals from a time interval spanning several kiloyears, or bioturbation. $\delta^{13}C_{cib}$ minima during glaciations which experienced relatively low sedimentation rates, such as MIS 10, MIS 12, and MIS 14, are comparable to minima observed in glacial-time sediments deposited at higher sedimentation rates, for example, MIS 2 and MIS 6 (Figure 3). As such, the amplitude of $\delta^{13}C_{cib}$ shifts on orbital timescales (i.e., multiple kiloyears) at site PC493 do not appear to have been considerably attenuated by low sedimentation rates.

3.3. Paleoproductivity Proxies

The TOC content in core PC493 is 0.4–0.9 wt. % at the core top and <0.1–0.2 wt. % down-core (Figure 2). $CaCO_3$ contents are highest during interglacials, typically reaching values of 35–45%, and much lower during glacials, at times reaching values as low as 2–6%. Ba/Ti values are also lower during glacials, often reaching values of <0.05 compared with interglacial highs of >0.2. Percent $CaCO_3$ and Ba/Ti within the sediments of PC493 show a strikingly similar pattern throughout the last 800 kyr (Figure 3), suggesting that percent $CaCO_3$ is primarily a function of past productivity at this core site.

4. Discussion

4.1. Paleoproductivity and Carbonate Preservation at Site PC493

Down-core TOC values at site PC493 are generally low (<0.1–0.2 wt %) when compared to typical values of 0.1–0.4 wt. % at other sites from the Amundsen Sea (Hillenbrand et al., 2002) and the western Antarctic Peninsula margin (Pudsey & Camerlenghi, 1998). This likely reflects a low flux of organic material to the seafloor combined with its poor preservation in the sediments (DeMaster & Ragueneau, 1996), consistent with the low sedimentation rates at this site. Organic particulate fluxes in the seasonal sea ice zone of the Amundsen Sea are greatly reduced during periods of persistent sea ice cover compared with open water conditions, owing to reduced primary biological productivity in surface waters (Kim et al., 2015). Given the proximity of site PC493 to the modern summer sea ice limit (Jacka, 1997), it can be assumed that the site experienced prolonged periods of persistent sea-ice cover in the past, and thus reduced supply of organic matter to the sea floor. Low organic matter content likely inhibited the establishment of an abundant benthic community and, along with the absence of infaunal foraminifera species such as *Uvigerina*, probably prevented deep bioturbation of the sediments in core PC493.

There is a positive correlation between $CaCO_3$ contents and Ba/Ti (Pearson's R^2 of 0.78; Figure S2) in the sediments of core PC493, indicating that the percent $CaCO_3$ reflects primarily biological productivity and that this productivity signal has not been substantially overprinted by carbonate dissolution. The lack of carbonate dissolution overprinting demonstrates that site PC493 remained above the lysocline throughout the last 800 kyr. The poor correlation (Pearson's $R^2 = 0.28$; Figure S2) between the $CaCO_3$ content and $\delta^{13}C_{cib}$ furthermore indicates that the $\delta^{13}C_{cib}$ signal records changes in water mass chemistry rather than local productivity effects (Mackensen et al., 1993) and demonstrates that carbonate dissolution has not affected the $\delta^{13}C_{cib}$ record.

4.2. Late Quaternary $\delta^{13}C$ at Site TPC493

Averaged LGM $\delta^{13}C_{cib}$ values are 0.29 ±0.16‰ for TC493 and 0.35 ±0.14‰ for PC493 and did not fall below -0.01‰ in either core at any point during the last glacial period. This is also the case for most previous glacial periods within core PC493: only during MIS 16 and at Termination 9 (TIX) did $\delta^{13}C_{cib}$ values fall below -0.2‰. At no point did they reach the very low values recorded in sediment cores from the deep Atlantic SO, where glacial $\delta^{13}C_{cib}$ values repeatedly reached <-1.0‰. There is a long-term trend toward more positive $\delta^{13}C_{cib}$ values recorded at PC493 during glacials, which may be part of a longer term 400-kyr cyclicity observed in global carbon isotope records (Wang et al., 2010). Interglacial maxima in $\delta^{13}C_{cib}$ do not show the same trend, but this may be obscured by the high $\delta^{13}C_{cib}$ values observed in the Holocene (as recorded in TC493) and MIS 11 (Figure 3), both of which are particularly strong interglacials globally (Lang & Wolf, 2011). Interglacial $\delta^{13}C_{cib}$ values do not show a marked increase following the Mid-Bruhnes Event (approximately 430 ka). This contrasts with the $\delta^{18}O_{cib}$ record of PC493, which demonstrates increased interglacial intensity after 430 ka. (Figure 3).

The most prominent $\delta^{13}C_{cib}$ minimum recorded at site PC493 occurs during early MIS 16, at the time of cool substage MIS 16c (Bereiter et al., 2015), which corresponds to substage 16.4 in other substage assignments (Railsback et al., 2015), when values as low as -0.6‰ are recorded. Coeval $\delta^{13}C_{cib}$ minima are also observed in other $\delta^{13}C_{cib}$ records from the SO and Pacific but are much less pronounced in records of NCW (Lisiecki, 2010; Figure 4c). This $\delta^{13}C_{cib}$ minima coincided with the lowest pCO_2^{atm} recorded in Antarctic ice cores throughout the last 800 kyr, 174–180 ppmv between 665 and 668 ka (Lüthi et al., 2008; using the AICC2012 chronology of Bazin et al., 2013; Figure 4b). δD measurements suggest that air temperatures at the EPICA Dome C ice core site during MIS 16c were as low as those during the peak glacial conditions

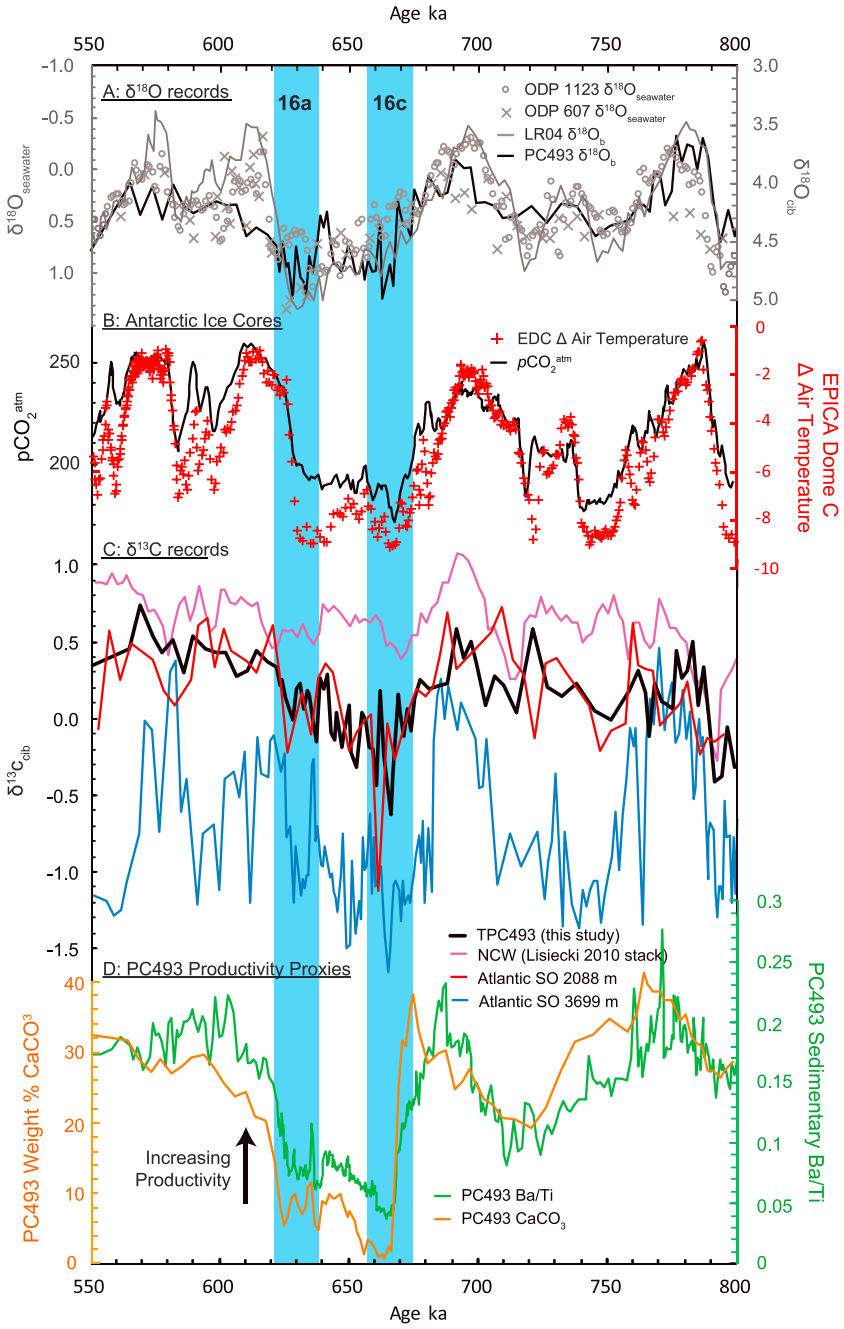

Figure 4. Paleoclimate proxy records spanning MIS 16. (a) $\delta^{18}O_b$ and $\delta^{18}O_{seawater}$ are characterized by gradual increases throughout MIS 16 (676–621 ka) followed by sharp decreases, reflecting the slow buildup and relatively rapid decay of northern hemisphere ice sheets (Elderfield et al., 2012; Ford et al., 2016; Lisiecki & Raymo, 2005; Sosdian & Rosenthal, 2009). (b) Peak pCO_2^{atm} values are reached relatively early, during MIS 16c, and coincide with minima in $\delta^{13}C_{cib}$ (c) recorded in the intermediate (red curve; Hodell et al., 2003) and deep (black and blue curves; this study; Hodell et al., 2003) Southern Ocean and a decrease in productivity (d: lower green and orange curves)—due to a seaward location of the summer sea ice limit—at site PC493. A stack of NCW $\delta^{13}C_{cib}$ records (c: magenta curve; Lisiecki, 2010) does not show the same extreme $\delta^{13}C_{cib}$ minimum during MIS 16c.

of MIS 16a, and comparable to other glacial minima (Jouzel et al., 2007; Figure 4b). The low $CaCO_3$ content and Ba/Ti ratios in sediments at site PC493 during the onset of MIS 16c (Figure 4d) reflect a drop in biological productivity, probably due to the summer sea ice limit being located north of the core site. This suggests the low air temperatures recorded in the EPICA Dome C ice core may have been part of a wider

early onset in extreme glacial conditions in the Antarctic region during MIS 16c. Seawater $\delta^{18}O$ reconstructions show no evidence for an expansion of northern hemisphere ice sheet during MIS 16c (Elderfield et al., 2012; Ford et al., 2016; Sosdian & Rosenthal, 2009; Figure 4a), suggesting that this climatic phenomenon was restricted to the southern hemisphere. The onset of the deposition of Heinrich Layers within the North Atlantic occurred later in MIS 16, suggesting that northern hemisphere intensification did occur later during MIS 16a (Hodell et al., 2008).

A $\delta^{13}C_{cib}$ minimum during MIS 16c is also evident in the cores of Ocean Drilling Program (ODP) Leg 177 Site 1088 (2,082-m water depth) and Site 1090 (3,699-m water depth) in the intermediate and deep Atlantic SO (Hodell et al., 2003), suggesting a SO-wide event. This ^{13}C depletion cannot be explained by a reduction in the end-member carbon isotope composition of NCW, which was similar to the onset of other glacials (Lisiecki, 2010; purple curve in Figure 4c). These $\delta^{13}C_{cib}$ data suggest a reduced supply of well-ventilated NCW to the SO, and thus a reduction in AMOC, and an expansion in SO-sourced deep waters depleted in ^{13}C. The perturbation in SO carbon chemistry during MIS 16c may reflect an increased storage of remineralized carbon within the deep ocean. If this were the case, a transfer of carbon from the atmosphere to the ocean interior would provide a mechanism to explain the pCO_2^{atm} minimum during MIS 16c.

4.3. $\delta^{13}C$ Values of SCW During the LGM

The persistent presence of SCW enriched in ^{13}C during the LGM and during previous glacial periods at site PC493 is at odds with previous studies of SO deep and bottom water masses, which largely describe heterogeneous, ^{13}C-depleted deep and bottom water masses within the glacial SO (e.g., Hodell et al., 2003; Mackensen et al., 2001; Ullermann et al., 2016; Venz & Hodell, 2002). To date, studies compiling global LGM $\delta^{13}C_{cib}$ data have largely either treated the intermediate to abyssal SO as one distinct water mass or failed to assess longitudinal differences in SO $\delta^{13}C_{cib}$ (compilations of Curry & Oppo, 2005; Oliver et al., 2010; Peterson et al., 2014). In light of our new $\delta^{13}C_{cib}$ data, we build upon previously published compilations to re-investigate the distribution of $\delta^{13}C_{\mathbf{cib}}$ data measured on *Cibicidoides* from core sites located south of 30°S.

The compiled LGM $\delta^{13}C_{cib}$ data are plotted as a function of water depth in supplementary Figure S3, however, due to the tilting of isopycnals within the SO as deep waters upwell around the Antarctic continent, water masses within the SO cannot always be defined by water depth alone. The LGM compilation of $\delta^{13}C_{cib}$ data is therefore also plotted as a function of the physical properties of waters bathing the core sites today in Figure 5. Although the physical properties of these waters varied in the past and were likely very different during the LGM, this is a useful visual aid to assess the potential sources and distribution of seawater DIC $\delta^{13}C$ of SO water masses. The compilation illustrates the difference in $\delta^{13}C_{cib}$ between core sites bathed today in LCDW/AABW (i.e., LGM SCW) from the Atlantic SO (Figure 5c) and the Pacific SO (Figure 5e). The lowest LGM $\delta^{13}C_{cib}$ values (dark blue/purple points in Figure 5) were all obtained from cores bathed in SCW within the Atlantic and Indian SO. One exception to this is core MD97-2121 (2,314-m water depth; average LGM $\delta^{13}C_{cib}$ = -1.09‰; McCave et al., 2008), which is located off the eastern coast of New Zealand in the SW Pacific and was apparently bathed in PDW during the LGM (McCave et al., 2008; Skinner et al., 2015). The LGM $\delta^{13}C_{cib}$ distribution in Figure 5 suggests that deep and bottom waters formed in the Atlantic SO south of the APF (i.e., the region where bottom waters are formed today) were the source of SCW with extremely low $\delta^{13}C$ values. In contrast to the Atlantic, there is a trend in the LGM Pacific SO data toward elevated $\delta^{13}C$ values within bottom water masses, with the lowest $\delta^{13}C_{cib}$ values found within cores bathed in CDW. This suggests the presence of bottom waters relatively better ventilated in the Pacific versus Atlantic SO.

Cores within the Atlantic SO that are today bathed in a mixture of CDW and NADW do not show the same level of ^{13}C depletion at the LGM as those bathed in deep and bottom waters (Figure 5c), suggesting a continued inflow of NCW (relatively well ventilated and low in remineralized nutrients, therefore relatively elevated in ^{13}C) to the SO. The pattern in the Indian SO is similar to that of the Atlantic SO, with SCW being depleted in ^{13}C, while cores that are bathed in UCDW or lie on a mixing line between UCDW and LCDW today were relatively enriched in ^{13}C (Figure 5d). This suggests the entrainment and advection of NCW into the intermediate-depth Indian SO continued during the LGM (Hu et al., 2016).

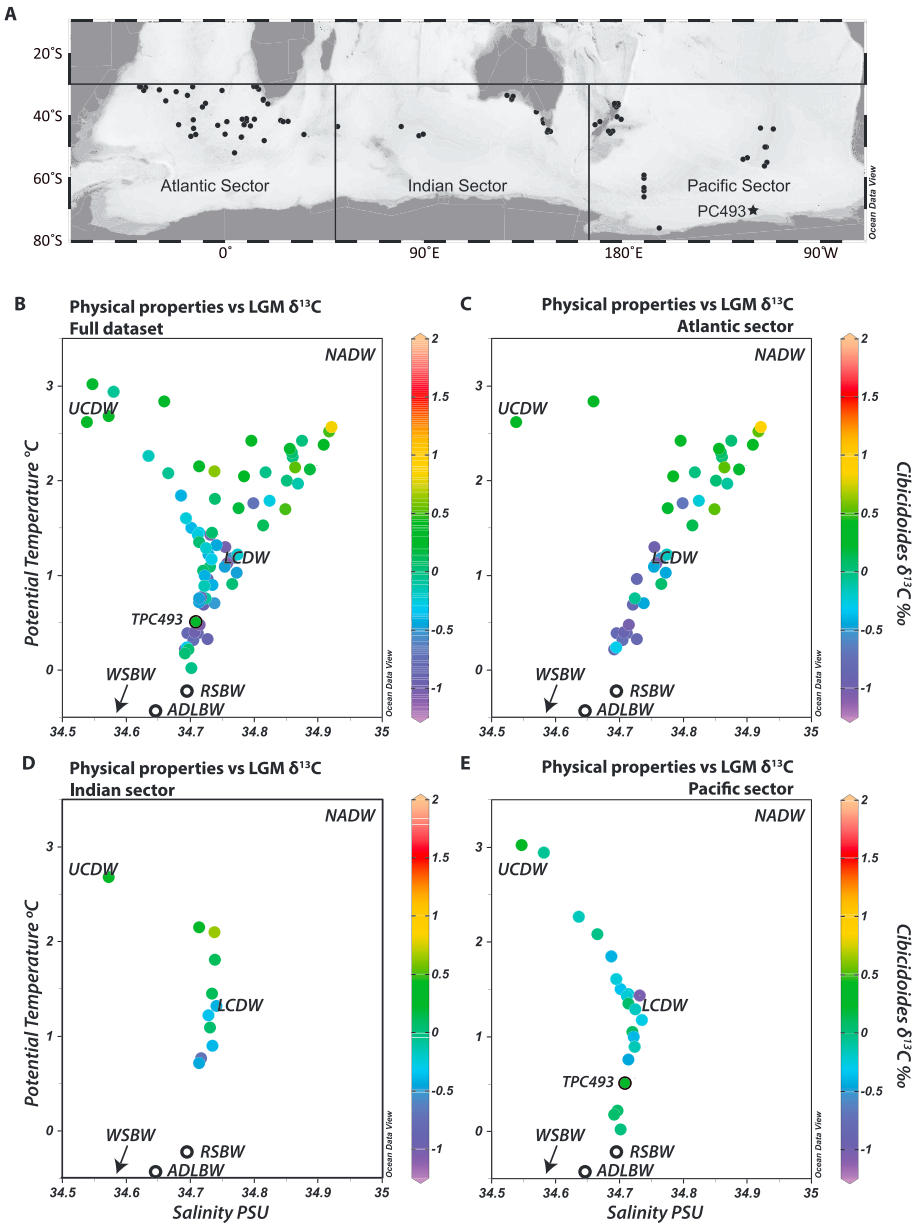

Figure 5. Average Last Glacial Maximum (LGM) $\delta^{13}C_{cib}$ values from *Cibicidoides* specimens as a function of the physical properties of modern deep and bottom water masses bathing the core sites. The $\delta^{13}C_{cib}$ compilation is after Peterson et al., 2014, with some additional data from the Pacific Southern Ocean (SO) and Pacific Ocean (Matsumoto et al., 2001; Molina-Kescher et al., 2016a; Ronge et al., 2015; Ullermann et al., 2016). See Table S2 for full list of data and references. (a) Core locations are shown and divided into (b) all core sites south of 30°S, (c) core sites in the Atlantic SO, (d) core sites in the Indian SO, and (e) core sites in the Pacific SO. Physical properties of water masses at core locations were compiled using the Hydrographic Atlas of the Southern Ocean (Olbers et al., 1992). Plots produced using Ocean Data View (Schlitzer, 2015). Cumulatively, Weddell Sea Bottom Water (WSBW; physical properties off the Y-axis in this figure), Adelie Land Bottom Water (ADLBW), Ross Sea Bottom Water (RSBW), and LCDW make up SCW at the LGM.

4.4. $\delta^{13}C$ of SCW During the Late Quaternary

In combination with other $\delta^{13}C_{cib}$ records from the SO, the $\delta^{13}C_{cib}$ record of PC493 allows us to infer spatial variations in deep water DIC $\delta^{13}C$ across the glacial-interglacial cycles of the past 800,000 years. The deep Pacific SO core sites E11-2 (3,109 m), PS75/059-2 (,3613 m), and PS75/056-1 (3,581 m) are all located far north of site PC493 on the East Pacific Rise in the central Pacific SO, north of the Subantarctic Front.

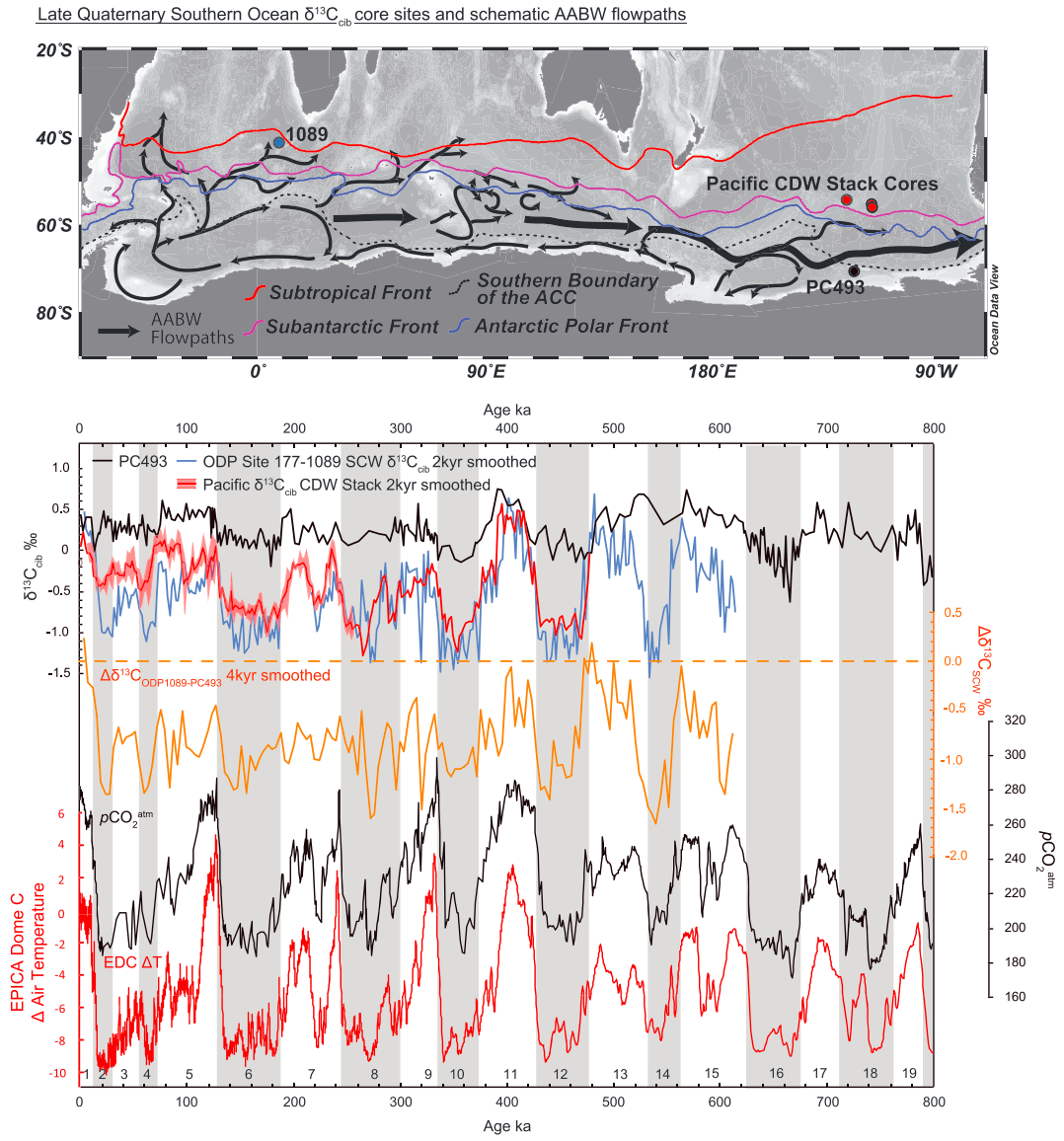

Figure 6. Comparison of the $\delta^{13}C_{cib}$ records of core PC493, Ocean Drilling Program (ODP) Leg 177 Site 1089, and a composite $\delta^{13}C_{cib}$ 'stack' of Circumpolar Deep Water (CDW) from the Pacific Southern Ocean produced by averaging and smoothing individual records at 2-kyr resolution (see text for references for records used for the stack). The red shading denotes 1σ error in this stack. The location of individual records is shown in the upper panel. The $\delta^{13}C_{cib}$ record from site PC493 and ODP 1089—bathed in SCW sourced in the high-latitude Atlantic Southern Ocean—were then both smoothed at 4-kyr resolution and the difference between them ($\delta^{13}C_{SCW}$) plotted. Increased spatial gradients in $\delta^{13}C_{SCW}$ coincide with periods of decreased pCO_2^{atm} and cooling of Antarctic air temperatures (EPICA Community Members, 2004; Jouzel et al., 2007).

These cores all record lower $\delta^{13}C_{cib}$ values than PC493 during past glacial periods (Figure 6; Ninnemann & Charles, 2002; Ullermann et al., 2016). These cores are today bathed in CDW and were located above the depth of AABW during at least the last glacial period (Basak et al., 2018). To explore the long-term trends in SO paleocirculation, we have smoothed these East Pacific Rise records to 2-kyr resolution and averaged them to form a 'stack' of central Pacific SO CDW of $\delta^{13}C$ (Figure 6). Ullermann et al. (2016) suggest that these East Pacific Rise core sites are bathed in CDW with a similar $\delta^{13}C$ composition as core sites located in the northern Cape Basin in the Atlantic SO, citing as evidence the near-identical evolution of $\delta^{13}C$ values between these locations (Ullermann et al., 2016). However, there exists a gradient between $\delta^{13}C$ values measured at these central Pacific SO sites and the deep southern Cape Basin, where $\delta^{13}C$ values

are consistently lower (e.g., ODP Leg 177 Site 1089 at 4,621-m water depth; Figure 6). This gradient is especially pronounced during past glacial periods and is attributed to the presence of AABW—sourced in the high-latitude Atlantic SO—within the southern Cape Basin, which was extremely ^{13}C-depleted during past glacials (Ullermann et al., 2016). This is consistent with the picture from the LGM, when deep core sites in the Atlantic SO were bathed in SCW with extremely negative $\delta^{13}C$ values. There exists throughout most of the last 614 kyr an even larger gradient in $\delta^{13}C$ between SCW bathing Site 1089 and SCW bathing site PC493. To investigate this gradient in high-latitude SCW $\delta^{13}C$, we have smoothed the $\delta^{13}C$ record of Site 1089 to 4-kyr resolution, to allow for direct comparison with the lower resolution $\delta^{13}C_{cib}$ record of core PC493. The record of PC493 has also been smoothed to a 4-kyr resolution, and the difference between these two smoothed records calculated. This allows us to directly gauge the spatial gradient in $\delta^{13}C$ of SCW sourced in the high-latitude Atlantic and Pacific SO ($\delta^{13}C_{SCW}$ in Figure 6).

Today, the SO is well mixed due to a combination of strong meridional and longitudinal circulation and intense diapycnal mixing, particularly in areas of rough bathymetry, such as the Scotia Sea in the Atlantic SO (Heywood et al., 2002). This mixing leads to the condensed temperature/salinity field observed in Figure 1c, and a homogenization of $\delta^{13}C$ DIC in the SO, which today averages 0.4±0.1‰ within CDW (Kroopnick, 1985). Conversely, a negative spatial gradient in $\delta^{13}C_{SCW}$ between the southern Cape Basin and high-latitude Pacific SO is apparent throughout much of the last 614 kyr (Figure 6), with the only exceptions being late MIS 15, late MIS 13, MIS 11, and the current interglacial. This suggests that the well mixed nature of the SO we observe today may not be the norm for the Late Quaternary, even during interglacial periods.

The largest gradient in $\delta^{13}C_{SCW}$ occurred during glacial periods, reflecting the ^{13}C depletion of SCW in the high-latitude Atlantic SO at these times. There is a close match between pCO_2^{atm} and $\delta^{13}C_{SCW}$, suggesting that $\delta^{13}C_{SCW}$ played a crucial role in regulating past pCO_2^{atm} concentrations (Figure 6), most likely through reduced ventilation and increased storage of respired carbon within SCW sourced within the Atlantic SO. It is also plausible, however, that changes in pCO_2^{atm} drove changes in bottom water formation, perhaps through cooling and expansion of grounded and floating ice in the formation regions, which in turn led to changes in physical properties of SCW and to reduced mixing between water masses, and hence a gradient in $\delta^{13}C_{SCW}$.

The presence of a gradient in $\delta^{13}C_{SCW}$ suggests that the water masses within the deep basins south of the APF in the Atlantic and Pacific SO were in the past more isolated from one another than in the modern ocean, especially during glacial periods (see Figure S4 for a schematic depiction of LGM water mass distributions). This increased isolation is in many ways unsurprising. In the modern SO, very little AABW formed in the Atlantic SO—if any—makes its way into the Pacific SO, rather it is mixed through the water column into overlying circumpolar deep water masses, which are then circulated throughout the SO via the ACC (Pardo et al., 2012). Where AABW (or modified AABW) does make its way between SO basins, it tends to do so via fracture zones, where strong diapycnal mixing between dense bottom waters and overlying water masses occurs (e.g., McCartney & Donohue, 2007). Temperature and salinity reconstructions suggest that LGM deep waters in the Atlantic SO were the densest waters in the global ocean (Adkins et al., 2002; Roberts et al., 2016). This high density was primarily driven by increased salinity, presumably acquired during SCW formation within the Atlantic SO, and led to a reduction in the mixing of this Atlantic SO sourced SCW into overlying circumpolar waters, which appears to have been a feature of past glaciations for at least the previous 500 kyr (Ullermann et al., 2016).

4.5. Implications for Deep Water Formation

The negative $\delta^{13}C_{cibs}$ values measured in the Atlantic SO and at core sites on the East Pacific Rise within the Pacific SO (Figure 6) suggest that some of the extremely ^{13}C-depleted AABW formed in the Atlantic SO during past glacial periods must have mixed with overlying CDW, and subsequently circulated though the SO and north in to the Atlantic, Indian, and Pacific oceanic basins (e.g., Figure S4). However, we argue based on measurements of SCW at site PC493 that deep waters forming within the high-latitude Pacific SO were not similarly ^{13}C-depleted. The development of the spatial gradient in $\delta^{13}C_{SCW}$ observed in Figure 6, especially pronounced during glacial periods, suggests differing mechanisms of deep- and bottom-water formation in the Atlantic and Pacific SO. While some of the glacial $\delta^{13}C_{cib}$ minima observed in the deep

Atlantic basin may have been related to PDW inflow to the SO (Ullermann et al., 2016), our new $\delta^{13}C_{cib}$ data excludes the region south of the APF in the Pacific SO as the source of an extremely ^{13}C-depleted, high-CO_2 water mass.

Some of the lowering of glacial seawater $\delta^{13}C$ values in the Subantarctic Zones of the Atlantic and Pacific SO may have been due to increases in biologically productivity driven by increased dust deposition during past glacial periods (Bradtmiller et al., 2009; Lamy et al., 2014; Martínez-Garcia et al., 2009, 2011), leading to increased remineralization of ^{12}C-rich organic matter at depth. However, the gradient in SCW $\delta^{13}C$ between the Atlantic and Pacific SO cannot be explained solely via productivity changes, as productivity increased in both the Pacific and Atlantic SO (Bradtmiller et al., 2009). Moreover, surface productivity in the region south of the APF actually decreased during past glacial periods (Bonn et al., 1998; Hillenbrand & Cortese, 2006; Jaccard et al., 2013; Nürnberg et al., 1997). As such, processes operating south of the APF within the Atlantic SO must have acted to reduce ventilation and maintain lowered $\delta^{13}C$ values. These processes probably include glacial changes in the production modes of deep and bottom waters, air-sea gas exchange (possibly linked to sea ice expansion), and vertical advection and/or mixing between SO water masses.

Today, most AABW within the Atlantic SO forms within the Weddell Sea. There, AABW precursor water masses are produced via two mechanisms: (i) brine rejection in regions of sea-ice formation and polynyas and (ii) supercooling of waters beneath floating ice shelves (Figure 7). The first mechanism leaves a high themodynamic imprint on AABW, leading to elevated $\delta^{13}C$ values (Mackensen, 2012), while the second mechanism minimizes this effect. Thus, increasing the relative proportion of bottom water production via supercooling beneath ice shelves in the past would act to decrease bottom water $\delta^{13}C$ compared to modern values. Hillenbrand et al. (2014) and Arndt et al. (2017) showed that due to widespread ice-sheet grounding the extent of floating ice shelves on the Weddell Sea embayment shelf at the LGM was smaller than at present, limiting or even preventing subice shelf formation of precursor water masses for SCW (Figure 17). If anything, this would lead to elevated bottom water $\delta^{13}C$ values compared with the modern, and therefore cannot explain the observed glacial depletion in ^{13}C of Atlantic SO SCW. Deep and bottom water formation via the process of brine rejection in polynyas north of regions of grounded ice could still have occurred during glacials (Mackensen et al., 1996; Smith et al., 2010). Brine rejection would also have provided the increased salinity required to drive an increased deep-shallow density contrast within the glacial SO (Ferrari et al., 2014). However, increasing the proportion of AABW precursor water mass formation via brine rejection in ice-free polynyas at the expense of production in subice shelf cavities would not have lessened the thermodynamic fractionation imprint on bottom water $\delta^{13}C$ compared to the modern and thereby cannot explain newly formed deep waters with very low $\delta^{13}C$ values (Mackensen, 2012; Mackensen et al., 1996, 2001). The answer to this paradox may lie in the glacial formation of AABW precursor water masses in the Atlantic SO by brine rejection under permanent sea-ice cover, thereby reducing the ability of thermodynamic fractionation during air-sea exchange to ventilate, or 'reset', the $\delta^{13}C$ of deep waters (Figure 7). Stephens and Keeling (2000) and Keeling and Stephens (2001) hypothesized that during past glacial periods, upwelling waters in the SO froze at the sea surface leading to increased winter and, at least locally, summer sea ice cover (Gersonde et al., 2005) and reduced air-sea gas exchange. A reduction in the transferal of deep water to the surface ocean, concurrent with the freshening of surface waters leading to the development of a stronger halocline across the MPT, has also been proposed as a mechanism for reducing ventilation of within the Antarctic Zone of the Atlantic SO during the Late Quaternary (Hasenfratz et al., 2019). This may not only have reduced surface ocean ventilation in the permanent sea-ice zone but also the seasonal sea-ice zone, where a fresh water lid prevented air-sea exchange (Hasenfratz et al., 2019; Mackensen, 2012). Lowering of CDW DIC $\delta^{13}C$ values due to increased remineralization of organic carbon north of the APF, as well as a decrease in the proportion of NADW with elevated $\delta^{13}C$ values entering the deep Atlantic SO, could not then be offset by air-sea gas exchange south of the APF during bottom water formation (Figure 7). As newly formed AABW circulated north of the APF, $\delta^{13}C$ may have been lowered by the further addition of remineralization of organic carbon, leading to the extremely low $\delta^{13}C_{cib}$ values recorded in the deep southern Cape Basin. In the modern Weddell Sea, mixing between CDW and newly formed bottom water 'dilutes' the $\delta^{13}C$ signature of bottom water masses, lessoning the gradient in $\delta^{13}C$ between CDW and AABW (Mackensen, 2012). The increased density of AABW during glacial periods compared with the modern would hinder this mixing, allowing the buildup of organic carbon within AABW and the lowering of seawater DIC $\delta^{13}C$ values beyond that of overlying CDW.

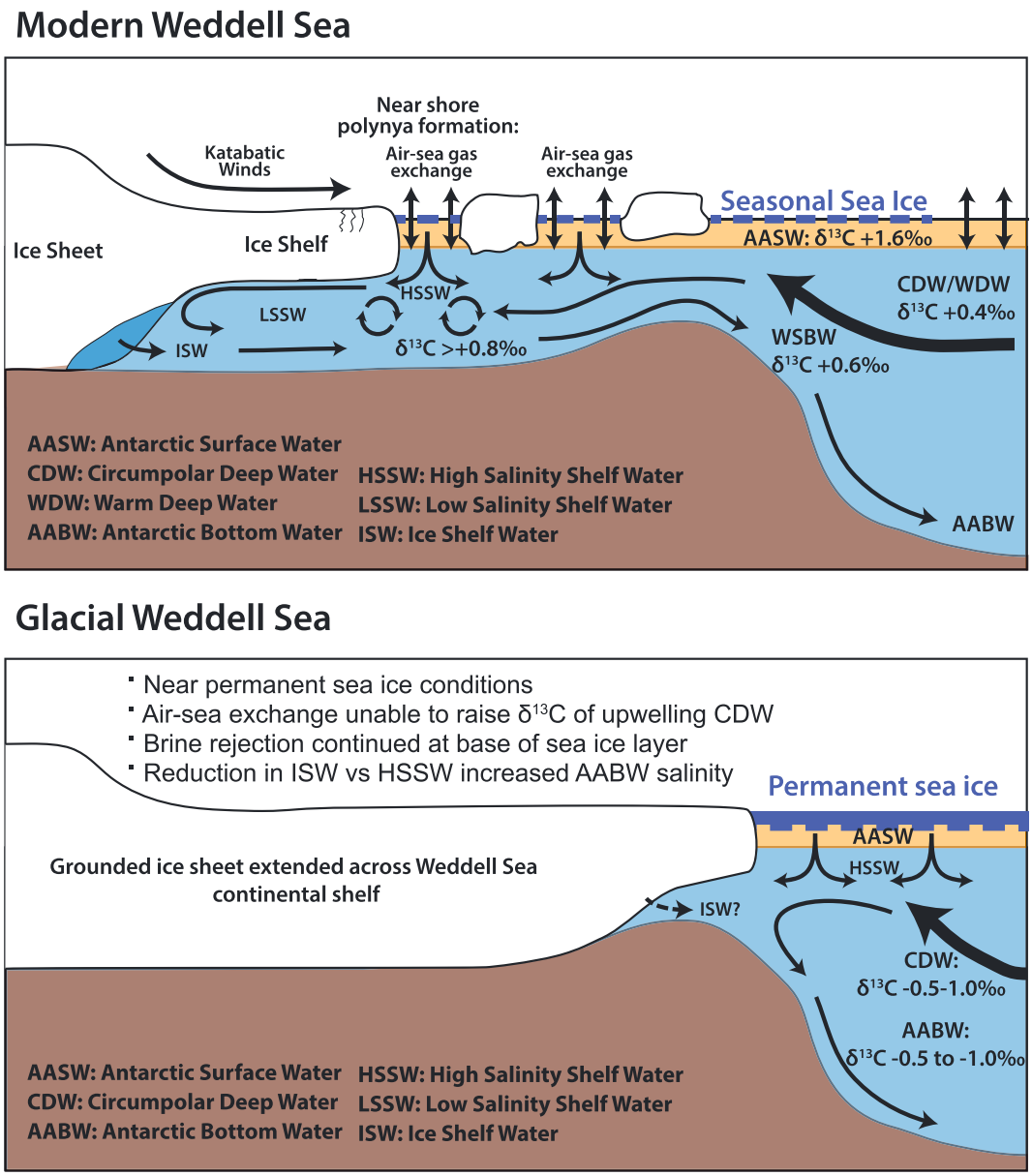

Figure 7. Schematic depiction of modern versus proposed glacial bottom water production mechanisms in the Weddell Sea. Modern Antarctic Bottom Water (AABW) $\delta^{13}C$ values ultimately reflect those of upwelling Circumpolar Deep Water (CDW) and recirculated Warm Deep Water (WDW), and Antarctic Surface Water (AASW), which undergoes buoyancy loss and sinks to form High Salinity Shelf Water (HSSW). Permanent or near-permanent sea ice conditions during glacials reduced or eliminated air-sea gas exchange during HSSW formation, restricting the ability of HSSW to 'reset' $\delta^{13}C$ of CDW/WDW toward higher values (Mackensen, 2012). Increased remineralization of organic carbon, coupled with decreased NADW (relatively high $\delta^{13}C$) contributions to CDW within the Atlantic Southern Ocean (SO), were thereby compounded by reduced bottom water ventilation, leading to extremely low $\delta^{13}C$ values of AABW within the Atlantic SO. In the Pacific SO, permanent sea ice may not have been as extensive (Benz et al., 2016) which, coupled with the presence of polynyas north of the Ross Sea shelf (Bonaccorsi et al., 2007; Smith et al., 2010), allowed for continued ventilation during bottom water production. Modern seawater $\delta^{13}C$ values in upper panel from Mackensen 2001, 2012, glacial seawater $\delta^{13}C$ estimates in lower panel from compilation in supplementary Table S2.

In contrast with the Atlantic SO, deep water formation mechanisms south of the APF in the Pacific SO maintained a relatively well-ventilated SCW, with elevated $\delta^{13}C$ values, even during glacial periods. In contrast to bottom water formation in the Weddell Sea, only a minor proportion of modern day Ross Sea Bottom Water production is attributed to the supercooling of waters beneath floating ice shelves, with the majority of AABW precursor water mass production occurring in the western Ross Sea Embayment via brine rejection during sea ice formation (Orsi & Wiederwohl, 2009). Reconstructed ice grounding limits within the

Ross Sea Embayment suggest that grounded ice expanded further north on the Ross Sea shelf at the LGM (Anderson et al., 2014), potentially further reducing the amount of deep water formation beneath floating ice shelves. The presence of polynyas over the north western Ross Sea continental slope has been inferred from the deposition of planktic foraminifera-bearing sediments (Bonaccorsi et al., 2007; Smith et al., 2010). LGM sea-ice reconstructions from the Pacific SO (Benz et al., 2016) show that in contrast to the Atlantic SO (Gersonde et al., 2005), the winter sea-ice limit there was only located slightly further north than today, making it less likely that AABW precursor water mass formation in the Ross Sea sector was maintained largely by brine rejection under permanent sea-ice cover, as may have been the case in the Weddell Sea (Mackensen, 2012). Thus, the surface waters, which went on to form AABW in the high-latitude Pacific SO, may have remained better ventilated than the Atlantic, with continued air-sea gas exchange and elevated $\delta^{13}C$ values, even during past glacial periods, ultimately leading to better ventilated bottom waters within the high-latitude Pacific SO, as observed at site PC493.

5. Conclusions

Today, the SO is relatively well mixed, leading to a small range of $\delta^{13}C$ DIC values between different SO water masses, with a SO average of ~0.4‰ (Kroopnick, 1985). During the LGM, a large difference in $\delta^{13}C_{cib}$ is observed between core sites bathed in SCW sourced from the Atlantic SO and site PC493 in the high-latitude Pacific SO. This difference is driven by a decrease in the $\delta^{13}C$ values of SCW forming in the Atlantic SO, where $\delta^{13}C_{cib}$ values of <-1.0‰ were repeatedly recorded during the last glacial period. In contrast, $\delta^{13}C_{cib}$ values in the high-latitude Pacific SO never fell below -0.01‰ during the last glacial period, reflecting the continued ventilation of SCW within this region.

A gradient in SCW $\delta^{13}C_{cib}$ values between the deep southern Cape Basin core site ODP 1089 and PC493 in the high-latitude Pacific SO is apparent throughout much of the last 614 kyr; however, it is most pronounced during glacial periods, when differences in $\delta^{13}C_{cib}$ of up to ~1.5‰ are observed. This suggests an increased isolation of bottom water masses within both the Atlantic and the Pacific (cf. McCave et al., 2008), consistent with increased bottom water densities (Adkins et al., 2002; Roberts et al., 2016) and decreased turbulent mixing (Ferrari et al., 2014) in the glacial Atlantic SO. This spatial gradient in SCW $\delta^{13}C$ values suggests differing modes of deep- and bottom-water formation in the Weddell Sea in the Atlantic SO versus the Pacific SO, especially during glacial periods. Changes in bottom-water formation in the Atlantic SO may have included a reduction in the formation of precursor water masses on the Antarctic continental shelf, or differences in the relative proportion of dense shelf waters formed under ice shelves versus those formed in polynyas. Evidence for increased salinity and an expansion of the seasonal sea ice zone in the Atlantic SO is consistent with increased deep-water formation via brine rejection during sea ice formation. This, however, would lead to an increase in the thermodynamic fractionation of carbon isotopes during air-sea gas exchange, increasing the $\delta^{13}C$ values of deep waters. This is the opposite of what is observed in the $\delta^{13}C_{cib}$ records from the Atlantic SO. It has been hypothesized that the formation of bottom waters via brine rejection under permanent sea-ice conditions, or in the seasonal sea-ice zone alongside the presence of a strongly stratified surface ocean covered by a freshwater 'lid', reduced this thermodynamic imprint on AABW forming in the Atlantic SO (Mackensen, 2012; Stephens & Keeling, 2000). In contrast, deep waters formed within the Pacific SO maintained elevated $\delta^{13}C$ values, most likely via continuous air-sea exchange.

The lowest $\delta^{13}C_{cib}$ values recorded in core PC493 occur during MIS 16c and coincide with minima in $\delta^{13}C_{cib}$ values in the intermediate and deep Atlantic SO, suggesting a SO-wide ^{13}C depletion at this time. This SO $\delta^{13}C$ minimum may have been driven by a prolonged expansion of poorly ventilated SCW combined with a reduced advection of NCW into the SO, and hence a reduction in the AMOC. This $\delta^{13}C$ minimum coincides with the lowest pCO_2^{atm} values observed in Antarctic ice cores, suggesting that a reduction in AMOC and/or ventilation of SCW within the SO may have played a role in the draw-down of pCO_2^{atm} at this time.

Acknowledgments
We thank the captain, crew, scientists, and support staff of expedition JR179 and Simon Crowhurst for performing XRF scanning of core PC493. T. J. W., C. D. H., C. S. A., and J. A. S. are supported by the Natural Environment Research Council (NERC). All data produced as part of this study are available in the supporting information and online in the Pangea database.

References

Adkins, J. F., McIntyre, K., & Schrag, D. (2002). The salinity, temperature, and $\delta^{18}O$ of the glacial deep ocean. *Science*, *298*, 1769–1773. https://doi.org/10.1126/science.1076252

Anderson, J. B., Conway, H., Bart, P. J., Witus, A. E., Greenwood, S. L., McKay, R. M., et al. (2014). Ross Sea paleo-ice sheet drainage and deglacial history during and since the LGM. *Quaternary Science Reviews*, *100*, 31–54. https://doi.org/10.1016/j.quascirev.2013.08.020

Anderson, R. F., Ali, S., Bradtmiller, L. I., Nielsen, S. H. H., Fleisher, M. Q., Anderson, B. E., & Burckle, L. H. (2009). Wind-driven upwelling in the Southern Ocean and the deglacial rise in atmospheric CO_2. *Science*, *323*, 1443–1448. https://doi.org/10.1126/science.1167441

Archer, D. E., Martin, P. a., Milovich, J., Brovkin, V., Plattner, G.-K., & Ashendel, C. (2003). Model sensitivity in the effect of Antarctic sea ice and stratification on atmospheric pCO_2. *Paleoceanography*, *18*(1), 1012. https://doi.org/10.1029/2002PA000760

Arndt, J. E., Hillenbrand, C. D., Grobe, H., Kuhn, G., & Wacker, L. (2017). Evidence for a dynamic grounding line in outer Filchner Trough, Antarctica, until the early Holocene. *Geology*, *45*, 1035–1038. https://doi.org/10.1130/G39398.1

Basak, C., Frollje, H., Lamy, F., Gersonde, R., Benz, V., Anderson, R. F., et al. (2018). Breakup of the last glacial deep stratification in the South Pacific. *Science*, *359*, 900–904. https://doi.org/10.1126/science.aao2473:

Bazin, L., Landais, A., Lemieux-Dudon, B., Toyé Mahamadou Kele, H., Veres, D., Parrenin, F., et al. (2013). An optimized multi-proxy, multi-site Antarctic ice and gas orbital chronology (AICC2012): 120-800 ka. *Climate of the Past*, *9*, 1715–1731. https://doi.org/10.5194/cp-9-1715-2013

Belanger, P. E., Curry, W. B., & Matthews, R. K. (1981). Core-top evaluation of benthic foraminiferal isotopic ratios for paleo-oceanographic interpretations. *Palaeogeography, Palaeoclimatology, Palaeoecology*, *33*, 205–220. https://doi.org/10.1016/0031-0182(81)90039-0

Benz, V., Esper, O., Gersonde, R., Lamy, F., & Tiedemann, R. (2016). Last Glacial Maximum sea surface temperature and sea-ice extent in the Pacific sector of the Southern Ocean. *Quaternary Science Reviews*, *146*, 216–237. https://doi.org/10.1016/j.quascirev.2016.06.006

Bereiter, B., Eggleston, S., Schmitt, J., Nehrbass-Ahles, C., Stocker, T. F., Fischer, H., et al. (2015). Revision of the EPICA Dome C CO_2 record from 800 to 600 kyr before present. *Geophysical Research Letters*, *42*, 542–549. https://doi.org/10.1002/2014GL061957

Bonaccorsi, R., Quaia, T., Burckle, L. H., Anderson, R. F., Melis, R., & Brambati, A. (2007). C-14 age control of pre- and post-LGM events using *N. pachyderma* preserved in deep-sea sediments (Ross Sea, Antarctica). In A. K. Cooper, C. R. Raymond, & the 10th ISAES Editorial Team (Eds.), *A Keystone in a Changing World*. Online Proceedings of the 10th ISAES X USGS Open-File Report 2007. Extended Abstract 098 (pp. 1–4). Washington, DC: National Academic Press.

Bonn, W. J., Gingele, F. X., Grobe, H., Mackensen, A., & Fütterer, D. K. (1998). Palaeoproductivity at the Antarctic continental margin: Opal and barium records for the last 400 ka. *Palaeogeography, Palaeoclimatology, Palaeoecology*, *139*, 195–211. https://doi.org/10.1016/S0031-0182(97)00144-2

Bostock, H. C., Barrows, T., Carter, L., Chase, Z., Cortese, G., Dunbar, G., et al. (2013). A review of the Australian–New Zealand sector of the Southern Ocean over the last 30 ka (Aus-INTIMATE project). *Quaternary Science Reviews*, *74*, 35–57.

Bradtmiller, L. I., Anderson, R. F., Fleisher, M. Q., & Burckle, L. H. (2009). Glacial to interglacial changes in the isotopic gradients of Southern Ocean surface water. *Paleoceanography*, *24*, PA2214. https://doi.org/10.1029/2008PA001693

Charles, C. D., & Fairbanks, R. G. (1990). Glacial to interglacial changes in the isotopic gradients of Southern Ocean surface water. In U. Bleil, & J. Thiede (Eds.), *Geological History of the Polar Oceans: Arctic versus Antarctic*, *NATO ASI Series (Series C: Mathematical and Physical Sciences)* (Vol. 308, pp. 519–538). Dordrecht: Springer. https://doi.org/10.1007/978-94-009-2029-3_30

Curry, W. B., & Oppo, D. W. (2005). Glacial water mass geometry and the distribution of $\delta^{13}C$ of ΣCO_2 the western Atlantic Ocean. *Paleoceanography*, *20*, PA1017. https://doi.org/10.1029/2004PA001021

DeMaster, D. J., & Ragueneau, O. (1996). Preservation efficiencies and accumulation ratesfor biogenic silica and organic C, N and P in high-latitude sediments: The Ross Sea. *Journal of Geophysical Research*, *101*, 18,501–18,518. https://doi.org/10.1029/96JC01634

Duplessy, J.-C., Shackleton, N. J., Matthews, R. K., Prell, W., Ruddiman, W. F., Caralp, M., & Hendy, C. H. (1984). ^{13}C Record of benthic foraminifera in the last interglacial ocean: Implications for the carbon cycle and the global deep water circulation. *Quaternary Research*, *21*, 225–243. https://doi.org/10.1016/0033-5894(84)90099-1

Elderfield, H., Ferretti, P., Greaves, M., Crowhurst, S. J., McCave, I. N., Hodell, D. A., & Piotrowski, A. M. (2012). Evolution of ocean temperature and ice volume through the Mid-Pleistocene climate transition. *Science*, *337*, 704–709. https://doi.org/10.1126/science.1221294

EPICA Community Members (2004). Eight glacial cycles from an Antarctic ice core. *Nature*, *429*, 623–628. https://doi.org/10.1038/nature02599

Ferrari, R., Jansen, M. F., Adkins, J. F., Burke, A., Stewart, A. L., & Thompson, A. F. (2014). Antarctic sea ice control on ocean circulation in present and glacial climates. *Proceedings of the National Academy of Sciences*, *111*, 8753–8758. https://doi.org/10.1073/pnas.1323922111

Ford, H. L., Sosdian, S. M., Rosenthal, Y., & Raymo, M. E. (2016). Gradual and abrupt changes during the Mid-Pleistocene Transition. *Quaternary Science Reviews*, *148*, 222–233. https://doi.org/10.1016/j.quascirev.2016.07.005

Freeman, E., Skinner, L. C., Waelbroeck, C., & Hodell, D. A. (2016). Radiocarbon evidence for enhanced respired carbon storage in the Atlantic at the Last Glacial Maximum. *Nature Communications*, *7*, 11998. https://doi.org/10.1038/ncomms11998

Garcia, H. E., Locarnini, R. A., Boyer, T. P., Antonov, J. I., Baranova, O. K., Zweng, M. M., et al. (2014). In S. Levitus, & A. Mishonov (Eds.), *World Ocean Atlas 2013, Volume 3: Dissolved oxygen, apparent oxygen utilization, and oxygen saturation*, NOAA Atlas NESDIS (Vol. *75*, p. 27).

Gebbie, G. (2014). How much did Glacial North Atlantic Water shoal? *Paleoceanography*, *29*, 190–209. https://doi.org/10.1002/2013PA002557

Gebbie, G., Peterson, C. D., Lisiecki, L. E., & Spero, H. J. (2015). Global-mean marine $\delta^{13}C$ and its uncertainty in a glacial state estimate. *Quaternary Science Reviews*, *125*, 144–159. https://doi.org/10.1016/j.quascirev.2015.08.010

Gersonde, R., Crosta, X., Abelmann, A., & Armand, L. (2005). Sea-surface temperature and sea ice distribution of the Southern Ocean at the EPILOG Last Glacial Maximum—A circum-Antarctic view based on siliceous microfossil records. *Quaternary Science Reviews*, *24*, 869–896. https://doi.org/10.1016/j.quascirev.2004.07.015

Graham, D., Corliss, B., Bender, M. L., & Keigwin, L. D. (1981). Carbon and oxygen isotopic disequilibria of recent deep-sea benthic foraminifera. *Marine Micropaleontology*, *6*, 483–497.

Hasenfratz, A. P., Jaccard, S. L., Martinez-Garcia, A., Sigman, D. M., Hodell, D. A., Vance, D., et al. (2019). The residence time of Southern Ocean surface waters and the 100,000-year ice age cycle. *Science*, *363*, 1080–1084. https://doi.org/10.1126/science.aat706

Hendry, K. R., Rickaby, R. E. M., Meredith, M. P., & Elderfield, H. (2009). Controls on stable isotope and trace metal uptake in *Neogloboquadrina pachyderma* (sinistral) from an Antarctic sea-ice environment. *Earth and Planetary Science Letters*, *278*, 67–77. https://doi.org/10.1016/j.epsl.2008.11.026

Heywood, K. J., Naveira Garabato, A. C., & Stevens, D. P. (2002). High mixing rates in the abyssal Southern Ocean. *Nature*, *415*, 1011–1014. https://doi.org/10.1038/4151011a

Hillenbrand, C.-D., Bentley, M. J., Stolldorf, T. D., Hein, a. S., Kuhn, G., Graham, A. G. C., et al. (2014). Reconstruction of changes in the Weddell Sea sector of the Antarctic Ice Sheet since the Last Glacial Maximum. *Quaternary Science Reviews*, *100*, 111–136. https://doi.org/10.1016/j.quascirev.2013.07.020

Hillenbrand, C.-D., & Cortese, G. (2006). Polar stratification: A critical view from the Southern Ocean. *Palaeogeography, Palaeoclimatology, Palaeoecology*, *242*, 240–252. https://doi.org/10.1016/j.palaeo.2006.06.001

Hillenbrand, C. D., Fütterer, D. K., Grobe, H., & Frederichs, T. (2002). No evidence for a Pleistocene collapse of the West Antarctic Ice Sheet from continental margin sediments recovered in the Amundsen Sea. *Geo-Marine Letters*, *22*, 51–59. https://doi.org/10.1007/s00367-002-0097-7

Hillenbrand, C.-D., Kuhn, G., & Frederichs, T. (2009). Record of a Mid-Pleistocene depositional anomaly in West Antarctic continental margin sediments: An indicator for ice-sheet collapse? *Quaternary Science Reviews*, *28*, 1147–1159. https://doi.org/10.1016/j.quascirev.2008.12.010

Hodell, D. A., Channell, J. E. T., Curtis, J. H., Romero, O. E., & Rohl, U. (2008). Onset of "Hudson Strati" Heinrich events in the eastern North Atlantic at the end of the middle Pleistocene transition (~640 ka)? *Paleoceanography*, *23*, PA4218. https://doi.org/10.1029/2008PA001591

Hodell, D. A., Venz, K. A., Charles, C. D., & Ninnemann, U. S. (2003). Pleistocene vertical carbon isotope and carbonate gradients in the South Atlantic sector of the Southern Ocean. *Geochemistry, Geophysics, Geosystems*, *4*(1), 1004. https://doi.org/10.1029/2002GC000367

Hoogakker, B. A. A., Elderfield, H., Schmiedl, G., McCave, I. N., & Rickaby, R. E. M. (2015). Glacial–interglacial changes in bottom-water oxygen content on the Portuguese margin. *Nature Geoscience*, *8*, 2–5. https://doi.org/10.1038/NGEO2317

Hu, R., Noble, T. L., Piotrowski, A. M., McCave, I. N., Bostock, H. C., & Neil, H. L. (2016). Neodymium isotopic evidence for linked changes in Southeast Atlantic and Southwest Pacific circulation over the last 200 kyr. *Earth and Planetary Science Letters*, *455*, 106–104. https://doi.org/10.1016/j.epsl.2016.09.027

Imbrie, J., Hays, J. D., Martinson, D. G., McIntyre, A., Mix, A. C., Morley, J. J., et al. (1984). The orbital theory of Pleistocene climate: support from a revised chronology of the marine $\delta^{18}O$ record. In A. Berger, *Milankovitch and Climate: Understanding the Response to Astronomical Forcing, Proceedings of the NATO Advanced Research Workshop held 30 November – 4 December, 1982* (Vol. 530, Part 1, pp. 269–305). Reidel Publishing.

Jaccard, S. L., Galbraith, E. D., Martínez-García, A., & Anderson, R. F. (2016). Covariation of deep Southern Ocean oxygenation and atmospheric CO_2 through the last ice age. *Nature*, *530*, 207–210. https://doi.org/10.1038/nature16514

Jaccard, S. L., Hayes, C. T., Martinez-Garcia, A., Hodell, D. A., Anderson, R. F., Sigman, D. M., & Haug, G. H. (2013). Two modes of change in Southern Ocean productivity over the past million years. *Science*, *339*, 1419–1423. https://doi.org/10.1126/science.1227545

Jacka, T.A., (1997). Antarctic CRC and Australian Antarctic Division Climate Data Sets [WWW Document]. URL http://www.antcrc.utas.edu.au/~jacka/climate.html

Jouzel, J., Masson-Delmotte, V., Cattani, O., Dreyfus, G., Falourd, S., Hoffmann, G., et al. (2007). Orbital and millennial Antarctic climate variability over the past 800,000 years. *Science*, *317*, 793–796. https://doi.org/10.1126/science.1141038

Keeling, R. F., & Stephens, B. B. (2001). Antarctic sea ice and the control of Pleistocene climate instability. *Paleoceanography*, *16*, 112–131. https://doi.org/10.1029/2000PA000529

Keigwin, L. D. (1998). Glacial-age hydrography of the far northwest Pacific Ocean. *Paleoceanography*, *13*, 323–339. https://doi.org/10.1029/98PA00874

Kim, M., Hwang, J., Kim, H. J., Kim, D., Yang, E. J., Ducklow, H. W., et al. (2015). Sinking particle flux in the sea ice zone of the Amundsen Shelf, Antarctica. *Deep-Sea Research I*, *101*, 110–117. https://doi.org/10.1016/j.dsr.2015.04.002

Kohfeld, K. E., Anderson, R. F., & Lynch-Stieglitz, J. (2000). Carbon isotopic disequilibrium in polar planktonic foraminifera and its impact on modern and Last Glacial Maximum reconstructions. *Paleoceanography*, *15*, 53–64. https://doi.org/10.1029/1999PA900049

Kohfeld, K. E., Fairbanks, R. G., Smith, S. L., & Walsh, I. D. (1996). *Neogloboquadrina Pachyderma* (sinistral coiling) as Paleoceanographic tracers in Polar Oceans: Evidence from Northeast Water Polynya Plankton Tows, Sediment Traps, and Surface Sediments. *Paleoceanography*, *11*, 679–699. https://doi.org/10.1029/96pa02617

Kroopnick, P. (1985). The distribution of ^{13}C of ΣCO_2 in the world oceans. *Deep Sea Research Part A. Oceanographic Research Papers*, *32*, 57–84. https://doi.org/10.1016/0198-0149(85)90017-2

Lamy, F., Gersonde, R., Winckler, G., Esper, O., Jaeschke, A., Kuhn, G., et al. (2014). Increased dust deposition in the Pacific Southern Ocean during glacial periods. *Science*, *343*, 403–407. https://doi.org/10.1126/science.1245424

Lang, N., & Wolf, E. W. (2011). Interglacial and glacial variability from the last 800 ka in marine, ice and terrestrial archives. *Climate of the Past*, *7*, 361–380. https://doi.org/10.5194/cp-7-361-2011

Lisiecki, L. E. (2010). A simple mixing explanation for late Pleistocene changes in the Pacific-South Atlantic benthic $\delta^{13}C$ gradient. *Climate of the Past*, *6*, 305–314. https://doi.org/10.5194/cp-6-305-2010

Lisiecki, L. E., & Raymo, M. E. (2005). A Pliocene-Pleistocene stack of 57 globally distributed benthic ^{18}O records. *Paleoceanography*, *20*, PA1003. https://doi.org/10.1029/2004PA001071

Lu, Z., Hoogakker, B. A. A., Hillenbrand, C., Zhou, X., Thomas, E., Gutchess, K. M., et al. (2016). Oxygen depletion recorded in upper waters of the glacial Southern Ocean. *Nature Comunications*, *7*, 11146. https://doi.org/10.1038/ncomms11146

Lund, D. C., Adkins, J. F., & Ferrari, R. (2011). Abyssal Atlantic circulation during the Last Glacial Maximum: Constraining the ratio between transport and vertical mixing. *Paleoceanography*, *26*, PA1213. https://doi.org/10.1029/2010PA001938

Lüthi, D., Le Floch, M., Bereiter, B., Blunier, T., Barnola, J. M., Siegenthaler, U., et al. (2008). High-resolution carbon dioxide concentration record 650,000-800,000 years before present. *Nature*, *453*, 379–382. https://doi.org/10.1038/nature06949

Lynch-Stieglitz, J., Adkins, J. F., Curry, W. B., Dokken, T., Hall, I. R., Herguera, J. C., et al. (2007). Atlantic Meridional Overturning during the Glacial Maximum. *Science*, *316*, 66–69. https://doi.org/10.1126/science.1137127

Mackensen, A. (2012). Strong thermodynamic imprint on Recent bottom-water and epibenthic $\delta^{13}C$ in the Weddell Sea revealed: Implications for glacial Southern Ocean ventilation. *Earth and Planetary Science Letters*, *317–318*, 20–26. https://doi.org/10.1016/j.epsl.2011.11.030

Mackensen, A., Hubberten, H.-W., Bickert, T., & Futterer, D. K. (1993). The $\delta^{13}C$ in benthic foraminiferal tests of *Fontbotia Wuellerstorfi* (Scwager) relative to the $\delta^{13}C$ of dissolved inorganic carbon in Southern Ocean Deep Water: implications for glacial ocean circulation models. *Paleoceanography*, *8*, 587–610. https://doi.org/10.1029/93PA01291

Mackensen, A., Hubberten, H.-W., Scheele, N., & Schlitzer, R. (1996). Decoupling of $\delta^{13}C\Sigma CO_2$ and phosphate in Recent Weddell Sea deep and bottom water: Implications for glacial Southern Ocean paleoceanography. *Paleoceanography*, *11*, 203–215. https://doi.org/10.1029/95PA03840

Mackensen, A., Rudolph, M., & Kuhn, G. (2001). Late Pleistocene deep-water circulation in the subantarctic eastern Atlantic. *Global and Planetary Change*, *30*, 197–229. https://doi.org/10.1016/S0921-8181(01)00102-3

Marchitto, T. M., Curry, W. B., Lynch-Stieglitz, J., Bryan, S. P., Cobb, K. M., & Lund, D. C. (2014). Improved oxygen isotope temperature calibrations for cosmopolitan benthic foraminifera. *Geochimica et Cosmochimica Acta*, *130*, 1–11. https://doi.org/10.1016/j.gca.2013.12.034

Martínez-Garcia, A., Rosell-Melé, A., Geibert, W., Gersonde, R., Masqué, P., Gaspari, V., & Barbante, C. (2009). Links between iron supply, marine productivity, sea surface temperature, and CO_2 over the last 1.1 Ma. *Paleoceanography*, *24*, PA1207. https://doi.org/10.1029/2008PA001657

Martínez-Garcia, A., Rosell-Melé, A., Jaccard, S. L., Geibert, W., Sigman, D. M., & Haug, G. H. (2011). Southern Ocean dust-climate coupling over the past four million years. *Nature*, *476*, 312–315. https://doi.org/10.1038/nature10310

Martinson, D. G., Stammerjohn, S. E., Iannuzzi, R. A., Smith, R. C., & Vernet, M. (2008). Western Antarctic Peninsula physical oceanography and spatio-temporal variability. *Deep Sea Research Part II: Topical Studies in Oceanography*, *55*, 1964–1987. https://doi.org/10.1016/j.dsr2.2008.04.038

Matsumoto, K., Lynch-Stieglitz, J., & Anderson, R. F. (2001). Similar glacial and Holocene Southern Ocean hydrography. *Paleoceanography*, *16*, 445–454. https://doi.org/10.1029/2000PA000549

McCartney, M. S., & Donohue, K. A. (2007). A deep cyclonic gyre in the Australian-Antarctic Basin. *Progress in Oceanography*, *75*, 675–750. https://doi.org/10.1016/j.pocean.2007.02.008

McCave, I. N., Carter, L., & Hall, I. R. (2008). Glacial–interglacial changes in water mass structure and flow in the SW Pacific Ocean. *Quaternary Science Reviews*, *27*, 1886–1908. https://doi.org/10.1016/j.quascirev.2008.07.010

McCorkle, D. C., Martin, P. A., Lea, D. W., & Klinkhammer, G. P. (1995). Evidence of a dissolution effect on benthic foraminiferal shell chemistry: $\delta^{13}C$, Cd/Ca, Ba/Ca, and Sr/Ca results from the Ontong Java Plateau. *Paleoceanography*, *10*, 699–714. https://doi.org/10.1029/95PA01427

Mix, A. C., Pisias, N. G., Zahn, R., Rugh, W., Lopez, C., & Nelson, K. (1991). Carbon 13 in Pacific Deep and Intermediate Waters, 0-370 ka: Implications for ocean circulation and Pleistocene CO_2. *Paleoceanography*, *6*, 205–226. https://doi.org/10.1029/90PA02303

Molina-Kescher, M., Frank, M., Tapia, R., Ronge, T. A., Nürnberg, D., & Tiedemann, R. (2016a). Reduced admixture of North Atlantic Deep Water to the deep central South Pacific during the last two glacial periods. *Paleoceanography*, *31*, 651–668. https://doi.org/10.1002/2015PA002863

Morozov, E. G., Demidov, A. N., Tarakanov, R. Y., & Zenk, W. (2010). Deep water masses of the South and North Atlantic. In E. G. Morozov, A. N. Demidov, R. Y. Tarakanov, & W. Zenk (Eds.), *Abyssal channels in the Atlantic Ocean: Water structure and flows*, (pp. 25–50). https://doi.org/10.1007/978-90-481-9358-5_2

Ninnemann, U. S., & Charles, C. D. (2002). Changes in the mode of Southern Ocean circulation over the last glacial cycle revealed by foraminiferal stable isotopic variability. *Earth and Planetary Science Letters*, *201*, 383–396. https://doi.org/10.1016/S0012-821x(02)00708-2

Nürnberg, C. C., Bohrmann, G., & Schltiter, M. (1997). Barium accumulation in the Atlantic sector of the Southern Ocean: Results from 190,000-year records. *Paleoceanography*, *12*, 594–603.

Olbers, D., Gouretski, V., Seiß, G., Schröter, J., (1992). Hydrographic Atlas of the Southern Ocean. Alfred Wegener Institute for Polar and Marine Research, Bremerhaven.

Oliver, K., Hoogakker, B. A. A., Crowhurst, S., Henderson, G. M., Rickaby, R. E. M., Edwards, N. R., & Elderfield, H. (2010). A synthesis of marine sediment core $\delta^{13}C$ data over the last 150 000 years. *Climate of the Past*, *6*, 645–673. https://doi.org/10.5194/cp-6-645-2010

Orsi, A. H., Johnson, G. C., & Bullister, J. L. (1999). Circulation, mixing, and production of Antarctic Bottom Water. *Progress in Oceanography*, *43*, 55–109. https://doi.org/10.1016/S0079-6611(99)00004-X

Orsi, A. H., Whitworth, T., & Jr, W. D. N. (1995). On the meridional extent and fronts of the Antarctic Circumpolar Current. *Deep Sea Research Part I: Oceanographic Research Papers*, *42*, 641–673.

Orsi, A. H., & Wiederwohl, C. L. (2009). A recount of Ross Sea waters. *Deep Sea Research Part II: Topical Studies in Oceanography*, *56*, 778–795. https://doi.org/10.1016/j.dsr2.2008.10.033

Pados, T., Spielhagen, R. F., Bauch, D., Meyer, H., & Segl, M. (2015). Oxygen and carbon isotope composition of modern planktic foraminifera and near-surface waters in the Fram Strait (Arctic Ocean) - a case study. *Biogeosciences*, *12*, 1733–1752. https://doi.org/10.5194/bg-12-1733-2015

Pardo, P. C., Pérez, F. F., Velo, A., & Gilcoto, M. (2012). Water masses distribution in the Southern Ocean: Improvement of an extended OMP (eOMP) analysis. *Progress in Oceanography*, *103*, 92–105. https://doi.org/10.1016/j.pocean.2012.06.002

Peterson, C. D., Lisiecki, L. E., & Stern, J. V. (2014). Deglacial whole-ocean $\delta^{13}C$ change estimated from 480 benthic foraminiferal records. *Paleoceanography*, *29*, 549–563. https://doi.org/10.1002/2013PA002552

Pudsey, C. J., & Camerlenghi, A. (1998). Glacial-interglaical deposition on a sediment drift on the Pacific margin of the Antarctic Peninsula. *Antarctic Science*, *10*, 286–308. https://doi.org/10.1017/S0954102098000376

Railsback, L. B., Gibbard, P. L., Head, M. J., Voarintsoa, N. R. G., & Toucanne, S. (2015). An optimized scheme of lettered marine isotope substages for the last 1.0 million years, and the climatostratigraphic nature of isotope stages and substages. *Quaternary Science Reviews*, *111*, 94–106. https://doi.org/10.1016/j.quascirev.2015.01.012

Roberts, J., Gottschalk, J., Skinner, L. C., Peck, V. L., Kender, S., Elderfield, H., et al. (2016). Evolution of South Atlantic density and chemical stratification across the last deglaciation. *Proceedings of the National Academy of Sciences*, *113*, 514–519. https://doi.org/10.1073/pnas.1511252113

Ronge, T. A., Steph, S., Tiedemann, R., Prange, M., Merkel, U., Nürnberg, D., & Kuhn, G. (2015). Pushing the boundaries: Glacial/interglacial variability of intermediate and deep waters in the southwest Pacific over the last 350,000 years. *Paleoceanography*, *30*, 23–38. https://doi.org/10.1002/2014PA002727

Ronge, T. A., Tiedemann, R., Lamy, F., Köhler, P., Alloway, B. V., De Pol-Holz, R., et al. (2016). Radiocarbon constraints on the extent and evolution of the South Pacific glacial carbon pool. *Nature Communications*, *7*, 1–11. https://doi.org/10.1038/ncomms11487

Schlitzer, R., 2015. Ocean Data View, http://odv.awi.de.

Schmitt, J., Schneider, R., Elsig, J., Leuenberger, D., Lourantou, A., Chappellaz, J., et al. (2012). Carbon isotope constraints on the deglacial CO_2 rise from ice cores. *Science*, *336*, 711–714. https://doi.org/10.1126/science.1217161

Schmittner, A., Bostock, H. C., Cartapanis, O., Curry, W. B., Filipsson, H. L., Galbraith, E. D., et al. (2017). Calibration of the Carbon Isotope Composition ($\delta^{13}C$) of Benthic Foraminifera. *Paleoceanography*, *32*, 512–530. https://doi.org/10.1002/2016PA003072

Shackleton, N. J. (1974). Attainment of isotopic equilibrium ocean water and the benthic foraminifera genus *Uvigerina*: Isotopic changes in the ocean during the last glacial. *Colloque international du CNRS*, *219*, 203–210.

Sikes, E. L., Allen, K. A., & Lund, D. C. (2017). Enhanced $\delta^{13}C$ and $\delta^{18}O$ differences between the South Atlantic and South Pacific during the Last Glaciation: The deep gateway hypothesis. *Paleoceanography*, *32*, 1000–1017. https://doi.org/10.1002/2017PA003118

Sikes, E. L., Cook, M. S., & Guilderson, T. P. (2016). Reduced deep ocean ventilation in the Southern Pacific Ocean during the last glaciation persisted into the deglaciation. *Earth and Planetary Science Letters*, *438*, 130–138. https://doi.org/10.1016/j.epsl.2015.12.039

Simstich, J., Sarnthein, M., & Erlenkeuser, H. (2003). Paired $\delta^{18}O$ signals of *Neogloboquadrina pachyderma* (s) and *Turborotalita quinqueloba* show thermal stratification structure in Nordic Seas. *Marine Micropaleontology*, *48*, 107–125. https://doi.org/10.1016/S0377-8398(02)00165-2

Skinner, L. C., McCave, I. N., Carter, L., Fallon, S., Scrivner, A. E., & Primeau, F. (2015). Reduced ventilation and enhanced magnitude of the deep Pacific carbon pool during the last glacial period. *Earth and Planetary Science Letters*, *411*, 45–52. https://doi.org/10.1016/j.epsl.2014.11.024

Skinner, L. C., Primeau, F., Freeman, E., De La Fuente, M., Goodwin, P. A., Gottschalk, J., et al. (2017). Radiocarbon constraints on the glacial ocean circulation and its impact on atmospheric CO_2. *Nature Communications*, *8*, 1–10. https://doi.org/10.1038/ncomms16010

Smith, J. A., Hillenbrand, C. D., Pudsey, C. J., Allen, C. S., & Graham, A. G. C. (2010). The presence of polynyas in the Weddell Sea during the Last Glacial Period with implications for the reconstruction of sea-ice limits and ice sheet history. *Earth and Planetary Science Letters*, *296*, 287–298. https://doi.org/10.1016/j.epsl.2010.05.008

Sosdian, S., & Rosenthal, Y. (2009). Deep-sea temperature and ice volume changes across the Pliocene-Pleistocene climate transitions. *Science*, *325*, 306–310. https://doi.org/10.1126/science.1169938

Stephens, B. B., & Keeling, R. F. (2000). The influence of Antarctic sea ice on glacial-interglacial CO_2 variations. *Nature*, *404*, 171–174. https://doi.org/10.1038/35004556

Talley, L. D. (2013). Closure of the global overturning circulation through the Indian, Pacific and Southern Oceans: Schematics and transports. *Oceanography*, *26*, 80–97. https://doi.org/10.5670/oceanog.2013.07

Ullermann, J., Lamy, F., Ninnemann, U. S., Lembke-Jene, L., Gersonde, R., & Tiedemann, R. (2016). Pacific-Atlantic Circumpolar Deep Water coupling during the last 500 ka. *Paleoceanography*, *31*, 639–650. https://doi.org/10.1002/2016PA002932

Venz, K. A., & Hodell, D. A. (2002). New evidence for changes in Plio-Pleistocene deep water circulation from Southern Ocean ODP Leg 177 Site 1090. *Palaeogeography, Palaeoclimatology, Palaeoecology*, *182*, 197–220. https://doi.org/10.1016/S0031-0182(01)00496-5

Wang, P., Tian, J., & Lourens, L. J. (2010). Obscuring of long eccentricity cyclicity in Pleistocene oceanic carbon isotope records. *Earth and Planetary Science Letters*, *290*, 319–330. https://doi.org/10.1016/j.epsl.2009.12.028

Woodruff, F., Savin, S. M., & Douglas, R. G. (1980). Biological fractionation of oxygen and carbon isotopes by recent benthic foraminifera. *Marine Micropaleontology*, *5*, 3–11. https://doi.org/10.1016/0377-8398(80)90003-1

Yu, J., Elderfield, H., & Piotrowski, A. M. (2008). Seawater carbonate ion-$\delta^{13}C$ systematics and application to glacial–interglacial North Atlantic ocean circulation. *Earth and Planetary Science Letters*, *271*, 209–220. https://doi.org/10.1016/j.epsl.2008.04.010

Yu, J., Menviel, L., Jin, Z. D., Thornalley, D. J. R., Barker, S., Marino, G., et al. (2016). Sequestration of carbon in the deep Atlantic during the last glaciation. *Nature Geoscience*, *9*, 319–324. https://doi.org/10.1038/ngeo2657

References From the Supporting Information

Bickert, T., & Mackensen, A. (2004). Last Glacial to Holocene changes in South Atlantic deep water circulation. In *The South Atlantic in the Late Quaternary* (pp. 671–693). Berlin Heidelberg: Springer.

Boyle, E. A. (1992). Cadmium and delta ^{13}C Paleochemical Ocean Distributions during the Stage 2 Glacial Maximum. *Annual Review of Earth and Planetary Sciences*, *20*, 245.

Carter, L., Manighetti, B., Ganssen, G., & Northcote, L. (2008). Southwest Pacific modulation of abrupt climate change during the Antarctic Cold Reversal-Younger Dryas. *Palaeogeography, Palaeoclimatology, Palaeoecology*, *260*, 284–298.

Charles, C. D., Froelich, P. N., Zibello, M. A., Mortlock, R. A., & Morley, J. J. (1991). Biogenic opal in Southern Ocean sediments over the last 450,000 years: Implications for surface water chemistry and circulation. *Paleoceanography*, *6*, 697–728.

Charles, C. D., Lynch-Stieglitz, J., Ninnemann, U. S., & Fairbanks, R. G. (1996). Climate connections between the hemisphere revealed by deep sea sediment core/ice core correlations. *Earth and Planetary Science Letters*, *142*, 19–27.

Charles, C. D., & Fairbanks, R. G. (1992). Evidence from Southern Ocean sediments for the effect of North Atlantic deep-water flux on climate. *Nature*, *355*, 416–419.

Curry, W. B., & Lohmann, G. P. (1982). Carbon isotopic changes in benthic foraminifera from the western South Atlantic: Reconstruction of glacial abyssal circulation patterns. *Quaternary Research*, *18*, 218–235.

Curry, W. B., & Lohmann, G. P. (1985). Carbon deposition rates and deep water residence time in the equatorial Atlantic Ocean throughout the last 160,000 years. In E. Sundquist, & W. Broecker (Eds.), *The Carbon Cycle and Atmospheric CO_2: Natural Variations Archean to Recent*, *Geophysics Monograph Series* (Vol. 32, pp. 285–301). Washington, DC: American Geophysical Union.

Curry, W. B., & Oppo, D. W. (2005). Glacial water mass geometry and the distribution of $\delta^{13}C$ of ΣCO_2 the western Atlantic Ocean. *Paleoceanography*, *20*, PA1017. https://doi.org/10.1029/2004PA001021

Curry, W. B., Duplessy, J., Labeyrie, L. D., & Shackleton, N. J. (1988). Changes in the distribution of $\delta^{13}C$ of deep water ΣCO_2 between the Last Glaciation and the Holocene. *Paleoceanography*, *3*, 317–341.

Govin, A., Michel, E., Labeyrie, L., Waelbroeck, C., Dewilde, F., & Jansen, E. (2009). Evidence for northward expansion of Antarctic Bottom Water mass in the Southern Ocean during the last glacial inception. *Paleoceanography*, *24*, PA1202. https://doi.org/10.1029/2008PA001603

Hodell, D. A., Curtis, J. H., Sierro, J., & Raymo, M. E. (2001). Correlation of late Miocene to early Pliocene sequences. *Paleoceanography*, *16*, 164–178.

Hodell, D. A., Venz, K. A., Charles, C. D., & Ninnemann, U. S. (2003). Pleistocene vertical carbon isotope and carbonate gradients in the South Atlantic sector of the Southern Ocean. *Geochemistry, Geophysics, Geosystems*, *4*(1), 1004. https://doi.org/10.1029/2002GC000367

Krueger, S., Leuschner, D. C., Ehrmann, W., Schmiedl, G., Mackensen, A., & Diekmann, B. (2008). Ocean circulation patterns and dust supply into the South Atlantic during the last glacial cycle revealed by statistical analysis of kaolinite/chlorite ratios. *Marine Geology*, *253*, 82–91.

Krueger, S., Leuschner, D. C., Ehrmann, W., Schmiedl, G., & Mackensen, A. (2012). North Atlantic Deep Water and Antarctic Bottom Water variability during the last 200ka recorded in an abyssal sediment core off South Africa. *Global and Planetary Change*, *80–81* 180, 189.

Lynch-Stieglitz, J., Fairbanks, R. G., & Charles, C. D. (1994). Glacial-interglacial history of Antarctic Intermediate Water: relative strengths of Antarctic versus Indian Ocean sources. *Paleoceanography*, *9*, 7–29.

Lynch-Stieglitz, J., Curry, W., & Oppo, D. (2006). Meridional overturning circulation in the South Atlantic at the last glacial maximum. *Geochemistry, Geophysics, Geosystems*, *7*, Q10N03. https://doi.org/10.1029/2005GC001226

Mackensen, A., Hubberten, H. W., Bickert, T., Fischer, G., & Fütterer, D. K. (1993). The $\delta^{13}C$ in benthic foraminiferal tests of *Fontbotia wuellerstorfi* (Schwager) relative to the $\delta^{13}C$ of dissolved inorganic carbon in southern ocean deep water: implications for glacial ocean circulation models. *Paleoceanography*, *8*, 587–610.

Mackensen, A., Grobe, H., Hubberten, H.-W., & Kuhn, G. (1994). Benthic foraminiferal assemblages and the $\delta^{13}C$-signal in the Atlantic sector of the Southern Ocean: Glacial-to-interglacial contrasts. In R. Zahn, et al. (Eds.), *Carbon Cycling in the Glacial Ocean: Constraints on the Ocean's Role in Global Change*, *NATO ASI Ser., Ser. I* (pp. 105–144). New York: Springer.

Mackensen, A., Rudolph, M., & Kuhn, G. (2001). Late Pleistocene deep-water circulation in the subantarctic eastern Atlantic. *Global and Planetary Change*, *30*, 197–229.

Marchitto, T. M., & Broecker, W. S. (2006). Deep water mass geometry in the glacial Atlantic Ocean: A review of constraints from the paleonutrient proxy Cd/Ca. *Geochemistry, Geophysics, Geosystems*, *7*, Q12003. https://doi.org/10.1029/2006GC001323

Martínez-Méndez, G., Molyneux, E. G., Hall, I. R., & Zahn, R. (2009). Variable water column structure of the South Atlantic on glacial–interglacial time scales. *Quaternary Science Reviews*, *28*, 3379–3387.

Matsumoto, K., & Lynch-stieglitz, J. (1999). Similar glacial and Holocene deep water circulation inferred from southeast Pacific benthic foraminiferal carbon isotope composition. *Paleoceanography*, *14*, 149–163.

Matsumoto, K., Lynch-Stieglitz, J., & Anderson, R. F. (2001). Similar glacial and Holocene Southern Ocean hydrography. *Paleoceanography*, *16*, 445–454.

McCave, I. N., Carter, L., & Hall, I. R. (2008). Glacial–interglacial changes in water mass structure and flow in the SW Pacific Ocean. *Quaternary Science Reviews*, *27*, 1886–1908.

McCorkle, D. C., Heggie, D. T., & Veeh, H. H. (1998). Glacial and Holocene stable isotope distributions in the southeastern Indian Ocean. *Paleoceanography*, *13*, 20–34.

McCorkle, D. C., Holder, A. L. (2001). Calibration Studies of Benthic Foraminiferal Isotopic Composition: Results from the Southeast Pacific. In AGU Fall Meeting Abstracts (Vol. 1, p. 0473).

Molina-Kescher, M., Frank, M., Tapia, R., Ronge, T. A., Nürnberg, D., & Tiedemann, R. (2016). Reduced admixture of North Atlantic Deep Water to the deep central South Pacific during the last two glacial periods. *Paleoceanography*, *31*, 651–668. https://doi.org/10.1002/2015PA002863

Molyneux, E. G., Hall, I. R., Zahn, R., & Diz, P. (2007). Deep water variability on the southern Agulhas Plateau: Interhemispheric links over the past 170 ka. *Paleoceanography*, *22*, PA4209. https://doi.org/10.1029/2006PA001407

Moy, A. D., Howard, W. R., & Gagan, M. K. (2006). Late Quaternary palaeoceanography of the Circumpolar Deep Water from the South Tasman Rise. *Journal of Quaternary Science*, *21*, 763–777.

Ninnemann, U. S., & Charles, C. D. (2002). Changes in the mode of Southern Ocean circulation over the last glacial cycle revealed by foraminiferal stable isotopic variability. *Earth and Planetary Science Letters*, *201*, 383–396.

Pahnke, K., & Zahn, R. (2005). Southern Hemisphere water mass conversion linked with North Atlantic climate variability. *Science*, *307*, 1741–1746.

Rau, A., Roger, J., Lutjeharms, J., Giraudeau, J., Lee-Thorp, J., Chen, M.-T., & Waelbroeck, C. (2002). A 450-kyr record of hydrological conditions on the western Agulhas Bank Slope, south of Africa. *Marine Geology*, *180*, 183–201.

Ronge, T. A., Steph, S., Tiedemann, R., Prange, M., Merkel, U., Nürnberg, D., & Kuhn, G. (2015). Pushing the boundaries: Glacial/interglacial variability of intermediate and deep waters in the southwest Pacific over the last 350,000 years. *Paleoceanography*, *30*, 23–38. https://doi.org/10.1002/2014PA002727

Sarnthein, M., Winn, K., Duplessy, J.-C., & Fontugne, M. (1988). Global variations of surface ocean productivity in low and mid latitudes: Influence on CO_2 reservoirs of the deep ocean and atmosphere during the last 21,000 years. *Paleoceanography*, *3*, 361–399.

Sarnthein, M., Winn, K., Jung, S. J., Duplessy, J. C., Labeyrie, L., Erlenkeuser, H., & Ganssen, G. (1994). Changes in east Atlantic deepwater circulation over the last 30,000 years: Eight time slice reconstructions. *Paleoceanography*, *9*, 209–267.

Sikes, E. L., Allen, K. A., & Lund, D. C. (2017). Enhanced $\delta^{13}C$ and $\delta^{18}O$ Differences Between the South Atlantic and South Pacific During the Last Glaciation: The Deep Gateway Hypothesis. *Paleoceanography*, *32*, 1000–1017. https://doi.org/10.1002/2017PA003118

Ullermann, J., Lamy, F., Ninnemann, U. S., Lembke-Jene, L., Gersonde, R., & Tiedemann, R. (2016). Pacific-Atlantic Circumpolar Deep Water coupling during the last 500 ka. *Paleoceanography*, *31*, 639–650. https://doi.org/10.1002/2016PA002932

Waelbroeck, C., Skinner, L. C., Labeyrie, L., Duplessy, J. C., Michel, E., & Vazquez Riveiros, N. (2011). The timing of deglacial circulation changes in the Atlantic. *Paleoceanography*, *26*, PA3213. https://doi.org/10.1029/2010PA002007